THESIS FOR THE DEGREE OF DOCTOR OF PHILOSOPHY IN THERMO AND FLUID DYNAMICS

Measurement and Evaluation of Near-field Spray Kinematics

For Nozzles with Asymmetrical Inlet Geometries

MOHAMMAD NIKOUEI

Department of Mechanics and Maritime Sciences

Division of Transport, Energy and Environment

CHALMERS UNIVERSITY OF TECHNOLOGY

Göteborg, Sweden 2025

Measurement and Evaluation of Near-field Spray Kinematics
For Nozzles with Asymmetrical Inlet Geometries
MOHAMMAD NIKOUEI
ISBN 978-91-8103-172-0

Doktorsavhandlingar vid Chalmers tekniska högskola
Ny serie nr. 5630
ISSN 0346-718X
Department of Mechanics and Maritime Sciences
Division of Transport, Energy and Environment
Chalmers University of Technology
SE-412 96 Göteborg
Sweden
Telephone: +46 (0)31-772 1000

Cover:
Sketch of a four-hole injector and fuel sprays

Chalmers Reproservice
Göteborg, Sweden 2025

Measurement and Evaluation of Near-field Spray Kinematics
For Nozzles with Asymmetrical Inlet Geometries
MOHAMMAD NIKOUEI
Department of Mechanics and Maritime Sciences
Division of Transport, Energy and Environment
Chalmers University of Technology

Abstract

This study digs into the complex dynamics and morphology of fuel sprays in diesel engines, with a special emphasis on the primary break-up phase. The main objective is to improve the basic knowledge of diesel fuel sprays by providing critical insights into their near-field behavior and velocity profiles. Furthermore, this study serves an additional purpose in providing statistical data required for validating computational spray models, which improves the accuracy of mixing and combustion simulation.

The core of this thesis is the investigation of near-field sprays, generated by nozzles with particular geometries at a range of injection pressures. The nozzles studied in this work include single-hole configurations with on-axis and off-axis orifices. In addition, a two-hole nozzle with angled orifices served as another case study. The study is based on optical measurements using time-gated ballistic imaging. This method provides clarity in identifying the liquid/gas interface and enables precise tracking of spray structures. This yields the temporal displacement of the spray interface between successive photos allowing the measurement of spray kinematics in two dimensions.

The findings highlight the major impact of asymmetrical inlet geometries on near-field spray profiles, introducing significant asymmetry in the distribution of velocity magnitude on either side of the spray. In addition, the investigation delves into the steady-state morphology of sprays for off-axis and two-hole nozzles. In the case of the off-axis nozzle, the spray deviates to the side with a sharper inlet edge, even at low injection pressures. The results show that this deviation is intensified with injection pressure. Furthermore, at higher pressures, the radial velocity component increases noticeably along the side with sharper orifice edges, resulting in a deviation of the spray axis.

The research also reveals details about velocity magnitude changes along the spray axis. The amplitude and frequency of these oscillations are significantly changed as injection pressure increases. Higher injection pressures cause greater amplitude in fluctuations, while the number of local peaks alongside the spray axis is decreased.

Finally, a comparison was made between simulated spray dynamics and the experimental data acquired throughout the project. The results of this comparative study show a notable agreement between the simulation model and the experimental data, particularly in cases with the empty sac as the initial condition (with 5% liquid fuel present in the sac before the start of injection). Here, the alignment in axial velocities shines out, while

small discrepancies in radial velocities are noted. This detailed comparison indicates the overall performance of the model, highlighting the strengths and limitations of the simulation model in capturing the complexities of spray behavior.

Keywords: Diesel Spray, Ballistic Imaging, Nozzle Geometry, Spray Dynamics

List of publications

The thesis is based on the work contained in the following publications:

Publication A M. Nikouei and D. Sedarsky, **Near-field spray velocity and development in single-hole diesel injector**, 31st Annual Conference on Liquid Atomization and Spray Systems, Madison, WI, May 2021

Publication B M.Nikouei and D.Sedarsky, **Effect of asymmetrical orifice inlet geometry on spray kinematics and development**, Fuel, 333, 2023

Publication C M. Nikouei and D. Sedarsky, **Effects of asymmetrical orifice inlet on steady-state diesel spray and the near-field kinematics** , 32nd Annual Conference on Liquid Atomization and Spray Systems, Naples, Italy, Sep 2023

Publication D M. Nikouei, D. Konstanzer, N. Giramondi, and D. Sedarsky, **Model Validation through Near-Field Spray Dynamics: A Case Study on Asymmetrical Off-axis Nozzle**, Journal of Atomization and Sprays, Vol. 35, 2025

Publication E M. Nikouei and D. Sedarsky, **Unveiling Spray Formation dynamics During Early Transient Injection**, Submitted to the Journal of Atomization and Sprays

Acknowledgements

I extend my sincere gratitude to Per Stålhammar, Magnus Pelz, and Niclas Wiker from Scania for initiating and facilitating this project. In addition, am very grateful for the invaluable supervision, support, and encouragement that I received from Dennis Konstanzer and Johan Linderyd, who gave me more confidence to continue this work.

I would like to thank my supervisor at the Chalmers University of Technology, Associate Prof. David Sedarsky, for his trust, support, and guidance. His belief in my abilities has been a driving force behind the success of this research endeavor.

I express my appreciation to Mats Andersson, my co-supervisor, whose insightful advice significantly contributed to the progress and quality of my research.

A special thanks to Nicola Giramondi, whose tips and guidance significantly expedited this project and helped me navigate through challenges. I also appreciate the support from Stefan Treutiger, who, along with Nicola, closely followed up on the design and fabrication of the injector holder.

The successful execution of my experiments owes much to the support of our dedicated lab engineers, Patrik Wåhlin and Alf Magnusson. Special mention goes to Anders Bragée for his excellent work in fabricating the injector mount, a crucial component for the experiments.

I am grateful to all the staff and colleagues at ECaPS (Pratheeba, Nidal, Christian, Lokesh, Mina, Morteza, Abhilash, Viktor, Yu, Magnus, and Ammar) for the nice moments and the wealth of knowledge shared. I will always remember the great moments that we spent together in the lunchroom, barbecue days, and Christmas time (Julbord) at Liseberg.

Last but not least, my heartfelt thanks to my parents my sisters, and my beloved Parichehr for supporting me anytime I needed them. Their encouragement has been a constant motivator on this journey, and I am grateful for their role in achieving this milestone.

Contents

1 Introduction

1.1 Motivation

To achieve sustainable development goals, expediting the advancement of vehicle powertrains, particularly in emission reduction, is vital and climate change remains a paramount global challenge. The prevailing scientific consensus emphasizes the escalating levels of greenhouse gas emissions, resulting in climate changes and undesired environmental impacts. At the heart of this issue is the need to mitigate emissions from various sources, including the transportation sector.

Studies show that the majority of goods transportation in Europe rely on road transportation, outstripping both water and rail. Predicted trends indicate that this dominance is likely to grow in the years to come[1]. In addition, the carbon dioxide (CO_2) emissions from trucks and buses are projected to rise by 2.2% annually, primarily attributed to the growing volume of transportation[2]. Nitrogen oxides (NO_x) and particulate matter (PM) constitute the primary pollutant emissions from heavy-duty vehicles, posing risks to public health and the environment. Consequently, there is a strong imperative to minimize the emissions of these vehicles to near-zero levels and address them through the adoption of advanced technologies [3].

In Compression Ignition (CI) engines, the cylinder draws in fresh air, which is then compressed by the piston movement. This compression elevates the temperature of the gas. Subsequently, when fuel is injected into this heated air, the subsequent combustion reaction raises the pressure within the combustion chamber, pushing the piston downward. In diesel engines, fuel injection occurs at exceptionally high pressure through relatively small nozzle openings of about hundreds μm. As the high-pressure fuel exits the nozzle orifices, it transforms into droplets and blends with the surrounding gas after evaporation. This mixing process can significantly affect the quality of combustion and the products.[4]. Accordingly, the fuel injection characteristics have a crucial effect on the mixing and combustion quality [5, 6, 7]. Hence, optimizing engine efficiency and reducing pollutant emissions is anticipated by fine-tuning fuel injection properties. However, pinpointing the ideal fuel injection characteristics poses challenges due to many parameters affecting the spray formation and mixing process. These parameters include nozzle geometry, injection pressure, ambient pressure, temperature, gas density, and fuel properties. Each parameter directly influences fuel spray characteristics, while their interactions add another layer of complications. In addition, the engine operates under variable load and speed conditions; therefore, some injection parameters, such as injection rate and pressure, will not remain constant. Notably, nozzle geometry holds particular significance among these parameters, as it dictates the distribution and targeting of fuel droplets. Numerous studies confirm that nozzle geometry significantly influences mixing and combustion characteristics [8, 9, 10, 11, 12]. Nevertheless, nozzle geometry is intricate, defined by multiple parameters like orifice diameter, conicity, cross-sectional shape, orifice length, number of orifices, and

orifice angle. This complexity adds challenges to identifying the optimal nozzle design for specific applications.

1.2 Objectives

Given the multitude of parameters influencing fuel injection and their varying impacts on combustion efficiency and quality, experimentally examining all possible combinations is prohibitively expensive and time-consuming. Consequently, computational simulations offer a cost-effective alternative for assessing the effects of different configurations. However, the precision of these simulations can occasionally be questionable, necessitating rigorous validation against experimental data. The level of model fidelity is determined by the simulation objectives, with trade-offs between accuracy and processing efficiency. It is essential to test these models based on experimental data to assure their reliability in real-world applications. The benefits of using a validated simulation model are enormous. It allows for conducting virtual experiments, eliminating the need for costly physical testing, and allows for the development of concepts that can significantly improve engine efficiency and reduce emissions.

The flow in the nozzle sac volume and near-field significantly influences fuel spray formation, playing a crucial role in fuel distribution and in-cylinder mixing conditions. This study aims to measure spray kinematics, focusing on fundamental knowledge for spray break-up, and understanding how inlet geometry impacts spray behavior across various operating conditions. The research also provides data for validating Computational Fluid Dynamics (CFD) models, contributing to the enhancement of mixing and combustion quality. The primary emphasis is on measuring near-field spray velocity, particularly with on-axis, off-axis, and two-hole geometries, to investigate the influence of interior and near-nozzle flows on spray morphology.

Accordingly, The first objective of this research is to look into the effect of nozzle geometry characteristics on the near-field spray. This investigation comprises a series of experiments with prototype injector nozzles, including three single-hole nozzles in addition to a two-hole nozzle. These nozzles differed in outlet diameter, conicity, orientation, and alignment. The work aims to unravel the correlation between geometrical characteristics and near-field spray behavior by experimental, analytical, and image-based diagnostic tools to measure the response of the near-field sprays in various test configurations. In addition, it is helpful to discover patterns and correlations between inlet geometry and spray morphology by measuring and comparing the penetration length, spray width, or cone angle for various conditions. the study attempts to find trends that will provide insights into the specific effects of inlet geometry on spray behavior. This analysis will enlighten the spray formation mechanics and provide useful information for optimizing injector design.

The impact of injection pressure on spray characteristics is another focus of the study,

which aims to determine which geometrical factors are more sensitive to pressure variations. To address this, experiments are conducted at various pressure levels, specifically 800, 1200, and 1600 bar. By systematically varying the injection pressure while keeping other parameters constant, the study aims to quantify the influence of pressure on key spray attributes. In addition, the research seeks to identify which spray characteristics are particularly influenced by the variation of injection pressure.

Finally, the study intends to evaluate the relationship between the nozzle's internal flow characteristics and the ensuing near-field spray. Visualizing the intricate flow patterns within the nozzle under realistic operating conditions poses a significant challenge, often necessitating specialized equipment such as X-ray imaging, which is not affordable in most cases. To address this challenge, the research endeavors to validate a simulation model using the data generated in this study. Upon successful validation, the simulation model can serve as a reliable tool to extract detailed information about the internal flow dynamics of the nozzle. This, in turn, enables a direct correlation to be established between the nozzle's internal flow behavior and the characteristics of the near-field spray. By bridging this gap between nozzle flow simulations and observed spray patterns, the study aims to provide valuable insights into the underlying mechanisms governing spray formation. This approach not only offers a cost-effective alternative to visualizing nozzle flow but also lays the foundation for a deeper understanding of the intricate interplay between nozzle geometry, internal flow dynamics, and near-field spray behavior.

2 Background

2.1 Diesel combustion

Diesel fuel contains long-chain hydrocarbon molecules that ignite rapidly in the presence of high-pressure and high-temperature air. The role of the fuel injection system in the diesel engine is metering and delivering a desired amount of fuel to the combustion chamber at a certain crank angle. In addition, the fuel must be distributed in the combustion chamber for efficient mixing with compressed air.

Diesel combustion is mixing controlled; in other words, the heat release rate and combustion efficiency are directly linked to characteristics of fuel atomization, evaporation, and mixing with air. In addition, the quantity of injected fuel controls the speed and torque in CI engines.

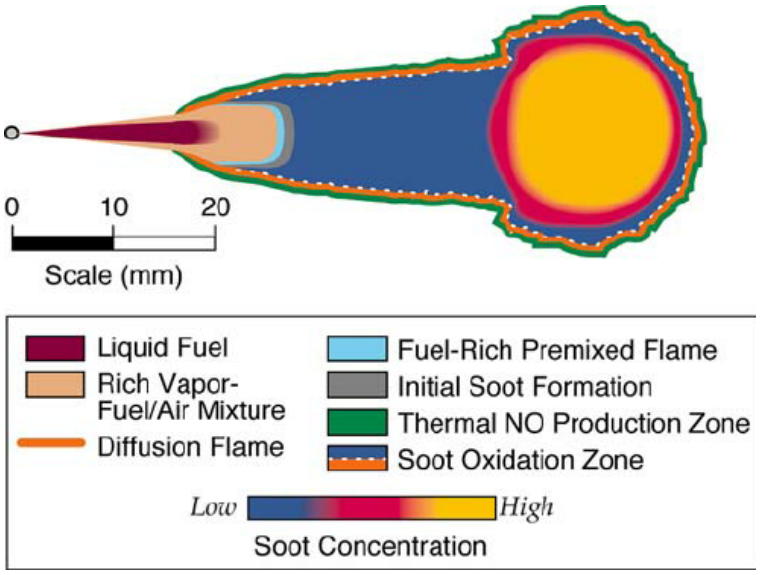

Figure 2.1: *Conceptual model for diesel combustion by J.D. Dec (adapted from [13])*

Unlike Spark Ignition (SI) engines, CI engines do not have special air/fuel ratio requirements. Diesel engines operate with heterogeneous mixture formation and auto-ignition, thus making it challenging to achieve an entirely homogeneous air-fuel mixture before or during the combustion. Consequently, the mixture in a diesel engine spans from $\lambda = 0$ (pure fuel) in the near-field spray to $\lambda = \infty$ (pure air) at the spray jet's outer edges. The excess-air factor (λ) quantifies the ratio of available air to the required air mass for stoichiometric combustion [14]. Furthermore, Compression Ignition (CI) engines generate significantly fewer unburned hydrocarbons (HC) and carbon monoxide (CO) compared to Spark Ignition (SI) engines, attributed to the ample oxygen in the combustion chamber. However, CI engines tend to produce higher levels of particulate matter (PM) due to non-uniform mixing and nitrogen oxides (NO_x) due to abundant

nitrogen and oxygen exposed to high temperatures. The DEC model [13] elucidates the pollutant formation process in diesel combustion. According to this model, soot primarily forms in the fuel-rich mixing zone, while NO_x is generated in the hotter reaction zones at the edge of the fuel plume. Consequently, the rate of soot formation and combustion is heavily influenced by the fuel-air mixing ratio and equivalence ratio. Conversely, NO_x is more likely to form on the outer surface, where the fuel-air mixture is lean. Balancing soot and NO_x formation necessitates optimal control of fuel-air mixing, highlighting the importance of establishing a trade-off between these pollutants.

2.2 Injection system

High injection pressure and fast responsive injectors with controlled discharge rates are desirable for increasing the efficiency and controllability of diesel engines. The common-rail system can vary injection timing and pressure over wide ranges. In this system, a rail accumulates fuel at high pressure, and injectors are fed by the rail through short pipes. The injectors are triggered and controlled by electrical signals and integrate the injection control valve and the atomizing nozzle. Thus injector and the nozzle unit are the key elements in this system [15].

2.2.1 Injector

In common-rail injection systems, the combination of injector needle dynamics and nozzle geometry specifies the quantity of the injected fuel and the structure of the diesel spray. Needle actuation and the transient hydraulics from the rail to the nozzle tip govern injection dynamics. The needle actuation is usually done in two general ways including solenoid-valve and piezo actuator. The piezoelectric injector presents faster needle opening and injection response than the solenoid injector [16, 17].

Figure 2.2(a) depicts the operation modes of the solenoid-valve injector. In this configuration, all cavities, including the control chamber, are filled with high-pressure fuel and create a positive pressure at the top of the needle to keep it close. When the solenoid coil is excited by an electrical signal, the solenoid armature moves upward, creating fuel flow from the valve control chamber to the cavity and the fuel tank through the return line. However, the inlet restrictor prevents a complete pressure compensation; thus, the valve-control chamber pressure falls below the nozzle chamber pressure. Therefore, the force acts on the control plunger and opens the nozzle needle. In order to stop the injection, the solenoid triggering signal is switched off. As a result, the valve spring presses the armature down, and the valve ball closes the outlet restrictor. Consequently, pressure in the control chamber rises again creating a greater force on the control plunger. The force on the valve-control chamber and the nozzle-spring force exceeds the force acting on the needle, closing the nozzle.

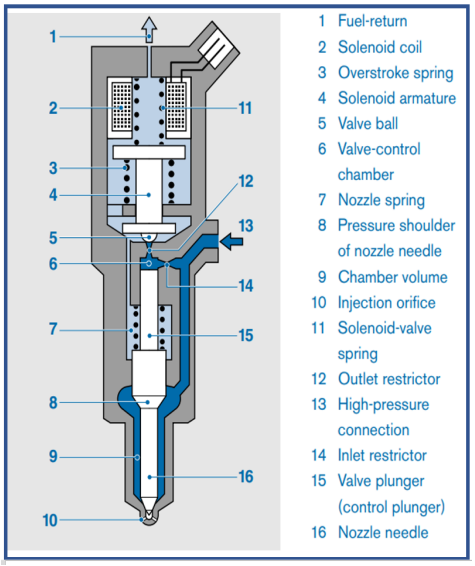

(a) Solenoid

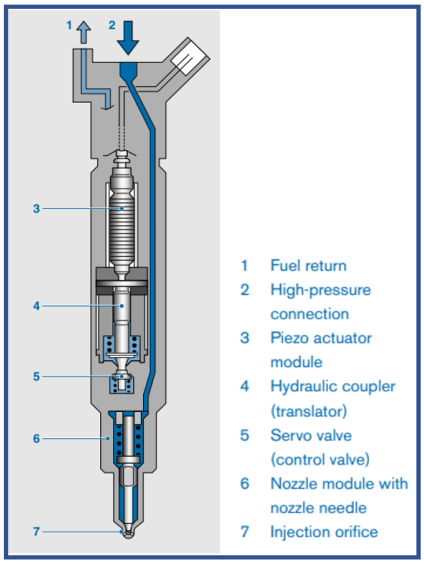

(b) Piezo

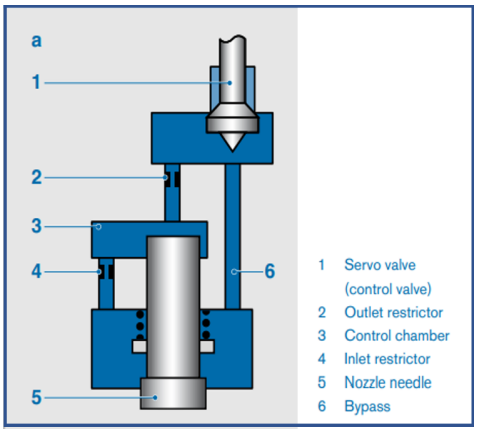

(c) Control-valve

Figure 2.2: *Common mechanisms for injector needle actuation (adapted from [18])*

The piezo actuator can improve injector stability and drift even further than solenoid systems because no mechanical force acts directly on the needle. In addition, this design reduces the moving masses and friction. It also provides a fast-responding injector with the capability of very short intervals between injection events. The working principle of this injector is similar to the solenoid-valve injector. However, the main difference between these two configurations is the control valve operation in the Piezo injector. Fig 2.2(b) illustrates the operation of the control valve. The rail pressure in the control chamber keeps the nozzle closed. When the piezo actuator is triggered, the servo valve opens and closes the bypass passage. The flow-rate ratio between the outlet and the inlet restrictors lowers the pressure in the control chamber, resulting in nozzle opening. The control volume flows via the servo valve to the low-pressure circuit of the overall system. For closing the nozzle, the servo valve releases the bypass passage. Thus, the inlet and

outlet restrictors reverse and refill the control chamber to raise its pressure. As soon as the required pressure is attained, the nozzle needle starts to move, and the injection process ends.

The injectors used for this research are of XPI (eXtra high Pressure Injection) type, developed and manufactured by Cummins. These injectors are capable of injection pressures up to 2400 bar. Fuel enters the cavity into the injector body from the side of the injector through the High-Pressure Connector (HPC). A typical XPI injector has three main modules: stator, control, and nozzle (Figure 2.3). The stator has an electromagnetic winding that pushes the armature plate upward in response to an electrical signal. The plunger movement causes a flow through the control valve, which lowers the pressure in the control chamber. As a result of the strong pressure gradients at both ends, the needle rises upward. As a result, the sac volume is filled with fuel, which exits through the nozzle holes, and injection begins. The springs force the plungers down and halt the flow as soon as the electrical signal is turned off.

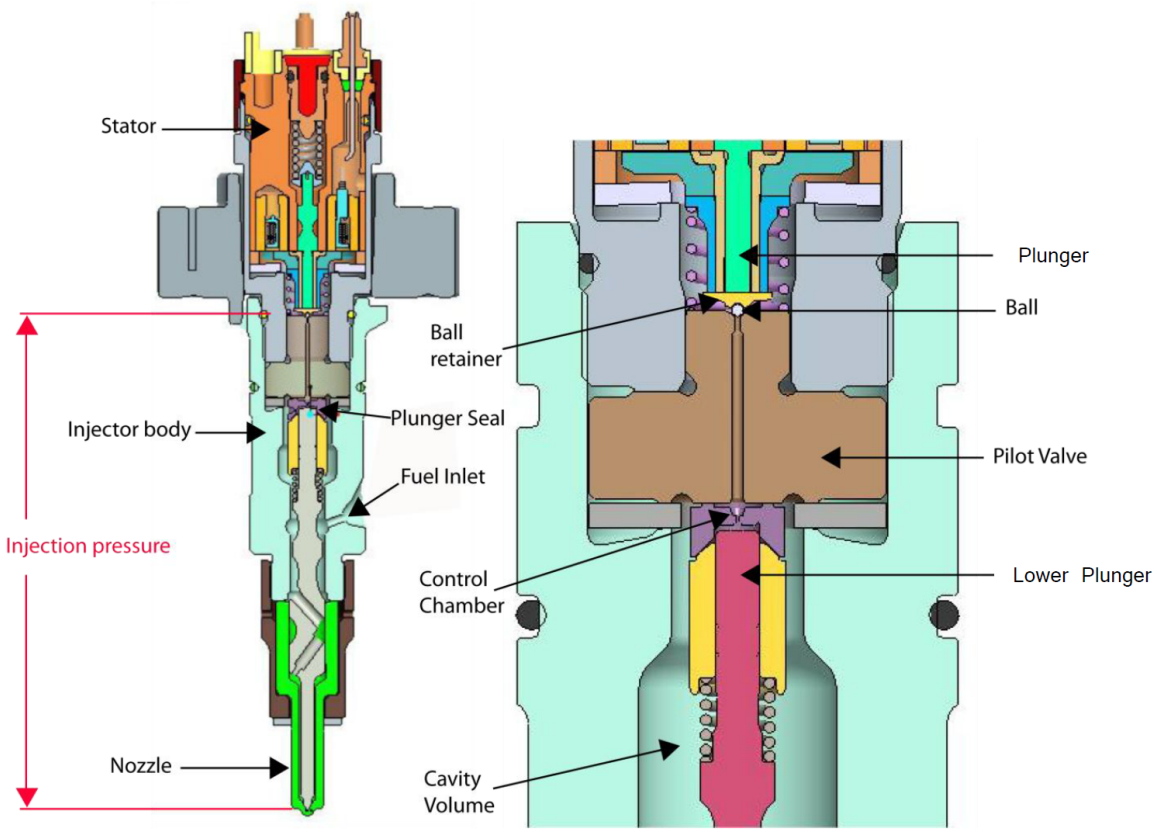

Figure 2.3: *Cross-section layout of an XPI injector and its main components.*

2.2.2 Nozzle

A typical injector has a nozzle with 8 to 12 holes (orifices) to distribute the fuel into the combustion chamber. Nozzle orifices can exist in various geometrical configurations.

The main parameters that are used to describe the orifice geometry include conicity, length-to-diameter ratio (L/D), orifice angle, and orifice position. Figure 2.4 depicts some of these parameters. In addition, the k-factor is a parameter to describe the conicity level of the orifice (equation 2.1). In this equation, D_i and D_o are the inlet and outlet diameters, respectively, and L is the length of the orifice. Thus, a positive k-factor implies a convergent orifice, whereas a negative number suggests a divergent orifice.

$$k_f = \frac{D_i - D_o}{10L} \tag{2.1}$$

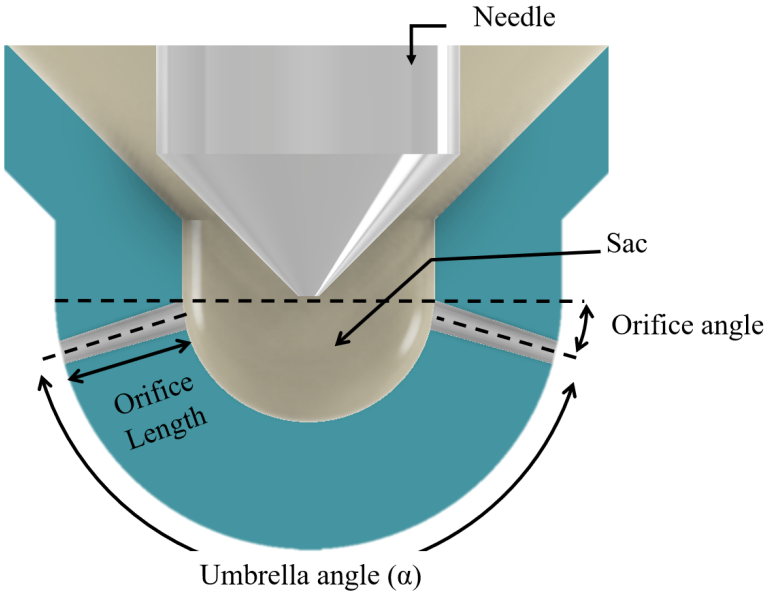

Figure 2.4: *A typical injector nozzle and its geometrical parameters*

The potential interactions between nozzle geometry and spray characteristics have been discussed in more detail in section 2.3.4.

2.3 Spray dynamics and instabilities

A fuel spray is defined as the finely atomized mist of fuel that is injected into the combustion chamber. In combustion engines, the fuel is injected in the form of a spray to promote evaporation and mixing of the fuel with air. In general, the spray formation and break-up are divided into primary and secondary break-up stages. Once the flow exits the nozzle orifice, a combined effect of instabilities including turbulence, cavitation, and aerodynamic forces, transforms the flow into ligaments and large droplets, often termed primary break-up. The secondary break-up is the process in which these large droplets break into smaller ones, and aerodynamic forces dominate this process in fuel injection sprays.

2.3.1 Turbulence

Turbulence is the main disturbance in the internal nozzle flow. Turbulence is generated by interactions between high-speed flow and surrounding walls, and it has a strong effect on primary breakup and surface wake growth. Reynolds (Re) number (equation 2.2) is the index of turbulence level in a flow so that a higher Reynolds number is equivalent to higher turbulence intensity. Reynolds number is defined as the ratio of inertial forces to viscous forces within a fluid:

$$Re = \frac{\rho.\nu.d}{\mu}, \tag{2.2}$$

where ρ is the fluid density, ν is flow velocity, μ is the fluid (fuel) viscosity, and d is the channel cross-sectional area, equivalent to orifice area for fuel injection application.

The flow characteristics at the nozzle exit are generally governed by the flow state upstream of the orifice and disturbances generated in the nozzle. For a given nozzle, the geometry parameters are constant, so the nature of the flow (laminar or turbulent) is dictated by the Reynolds number and velocity. In other words, there are links between nozzle geometry, the internal flow characteristics, and the near-field spray dynamics that affect break-up characteristics. For instance, if the flow at the orifice is fully turbulent, the radial velocity component leads to disruption of the surface film, followed by a general disintegration of the jet. In the case of fully turbulent flow, no aerodynamic forces are required for the break-up. Even when injected into a vacuum, the jet will disintegrate solely under the influence of turbulence [19, 20].

As soon as the flow leaves the nozzle and the physical constraint of the nozzle wall is removed, the velocity profile relaxation occurs by a mechanism of momentum transfer between transverse layers within the jet flow. This change in velocity profile that occurs downstream of the nozzle exit can influence the stability of the jet and its subsequent break-up into drops [19, 21].

In general four regimes of breakup are encountered as the liquid injection velocity is progressively increased [22]. Figure 2.5 indicates these regimes, encompassing the Rayleigh mechanism, first wind-induced, second wind-induced, and atomization regimes. The diameter of the produced droplets characterizes these regimes. In addition, the diagram shows that the jet instabilities can be characterized by Ohnesorge (Oh) and Reynolds numbers. The Ohnesorge number (Oh) relates the viscous forces to inertial and surface tension forces and can be written as equation 2.3:

$$Oh = \frac{\mu}{\sqrt{\rho.\sigma.d}}, \tag{2.3}$$

where μ is the fluid (fuel) viscosity, ρ is the fluid density, σ is the surface tension of the fluid, and d is the characteristic jet diameter, equivalent to orifice area for fuel injection

application.

Accordingly, the characteristics of the primary break-up can be classified by non-dimensional numbers such as Reynolds (equation 2.2), and Ohnesorge (equation 2.3).

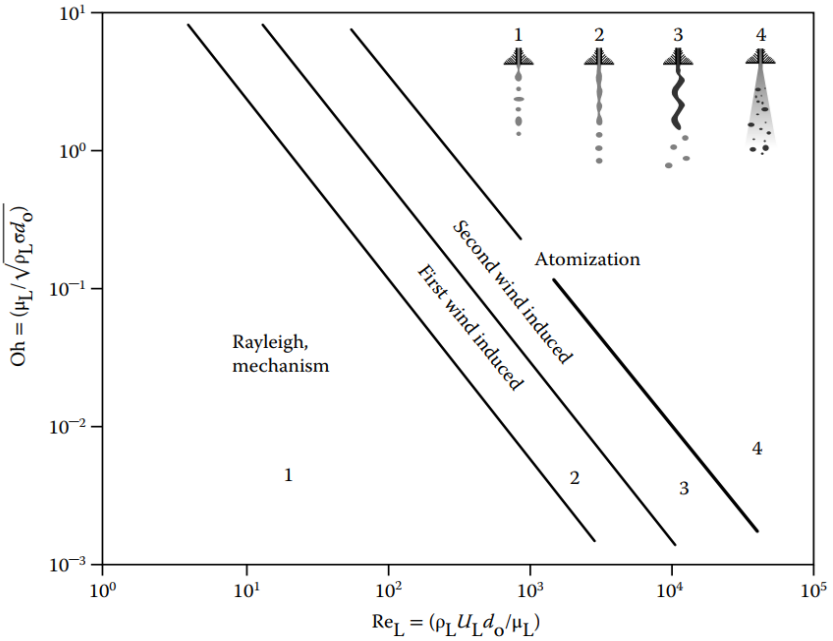

Figure 2.5: *Primary break-up classification diagram [19]*

2.3.2 Aerodynamics force

Among the break-up regimes mentioned in Figure 2.5, fuel injection in diesel engines is classified as the atomization break-up regime, which is correlated with extreme jet velocities. Therefore, aerodynamic interactions at the liquid/gas interface appear to be another major component of the break-up mechanism in this regime, producing droplets whose average diameter D is much smaller than the nozzle diameter. This process is often referred to as the secondary break-up.

The breakup of a droplet in a jet flow is governed by dynamic pressure, surface tension, and viscous forces. In most cases, the ratio of the aerodynamic forces and the surface tension forces determine the deformation of a drop. The ratio of these two opposing forces is known as the Weber (We) number (equation 2.4), which is another non-dimensional number to characterize the secondary break-up mechanism [23, 24]. The higher the Weber number, the more significantly the deforming pressure forces are compared with the reforming surface tension forces. In addition, a particular range of Weber numbers dictates specific breakup mechanisms, as depicted in Figure 2.6.

$$We = \frac{\rho.\nu^2.d}{\sigma}, \tag{2.4}$$

where ρ is the fluid density, ν is flow velocity, d is the flow cross-sectional area, and μ is the fluid viscosity.

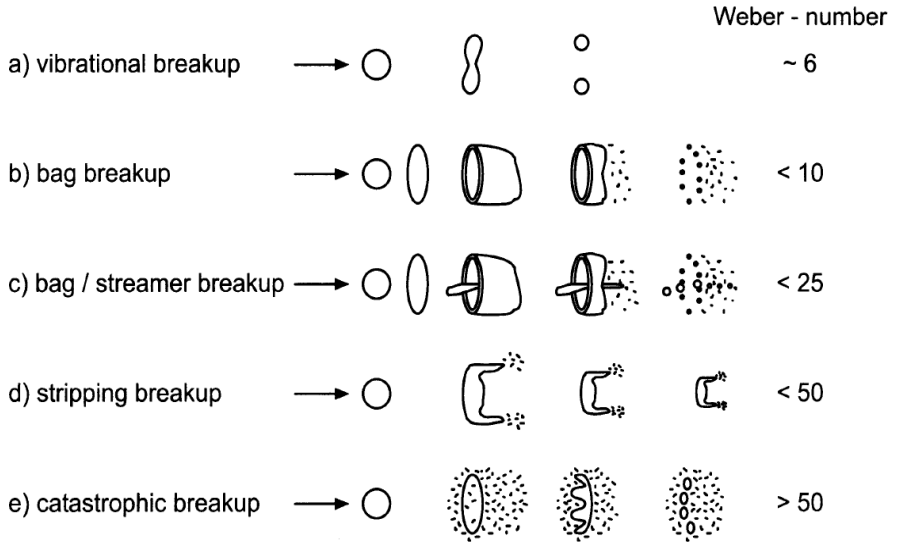

Figure 2.6: *Secondary break-up mechanisms classified by Weber number [23]*

Since the fuel jet atomizes into droplets of different dimensions, a mean diameter has to be defined to characterize the break-up quality. For this purpose, the so-called Sauter Mean Diameter (SMD) is used. The SMD is defined as the diameter of a droplet with the same volume/surface area ratio of the fuel jet. The atomization and evaporation of fuel improve if SMD decreases because the required time for evaporating a spherical droplet is proportional to the droplet diameter. This improvement can be achieved by smaller nozzle diameters, higher injection pressures, lower fuel viscosity, and surface tension.

2.3.3 Cavitation

When the local pressure in a liquid stream drops below the fluid's vapor pressure, vapor bubbles are formed, and this phenomenon is called cavitation. Cavitation usually occurs in applications involving high pressure gradients such as pump impellers, marine propellers, and fuel injectors. The vapor bubbles will collapse quickly upon their formation; the explosion of bubbles will induce high pressures on the contact surfaces, which has a destructive effect on surfaces in the long term. Although cavitation can be harmful to the nozzle hole structure, it can enhance atomization and prevent deposits from forming in the nozzle [25]. In addition, it can generate more dispersed sprays and improve air/fuel mixing [26].

The cavitation number is used as an index to characterize the potential for cavitation in a fluid flow, This number is dimensionless, which is defined as:

$$Ca = \frac{P_{\text{min}} - P_{\text{vapor}}}{0.5 \cdot \rho \cdot V^2} \tag{2.5}$$

where P_{min} is the minimum pressure in the flow, P_{vapor} is the vapor pressure of the liquid, ρ is the density of the liquid, and V is the velocity of the liquid.

The fuel flows at high pressures inside the injector nozzle, and this flow exits from tiny orifice holes. When the fuel comes in contact with the relatively sharp edges at the orifice inlet, a separation of the boundary layer from the orifice wall occurs, and it creates so-called "vena contracta" (Figure 2.7), which includes a recirculation zone [27]. As Figure 2.7 illustrates, the cross-sectional area becomes smaller, resulting in smaller effective area [28, 29, 30] . In addition, the velocity of the flow increases as a consequence of the reduction in friction between the flow and the internal orifice wall [29, 30]. Accordingly, the acceleration of flow causes pressure depression. If the pressure drop is significant enough, cavitation occurs, and vapor bubbles appear. As the edge radius gets smaller, the probability of cavitation occurrence becomes more significant [31]. Observations indicate that the discharge coefficient decreases as cavitation progresses but increases once the hydraulic flip occurs [32]. The hydraulic flip occurs when air at the nozzle exit extends back into the vena contracta region, leading to a smooth, laminar flow and sharp decrease in spray cone angle [33].

Cavitation intensity and form are varied during the injection stage, affected mainly by needle lift [32, 33, 34]. The cavitation can also occur at the needle tip, especially at low needle lift while the cavitation at the orifice inlet becomes more dominant at high needle lift [35].

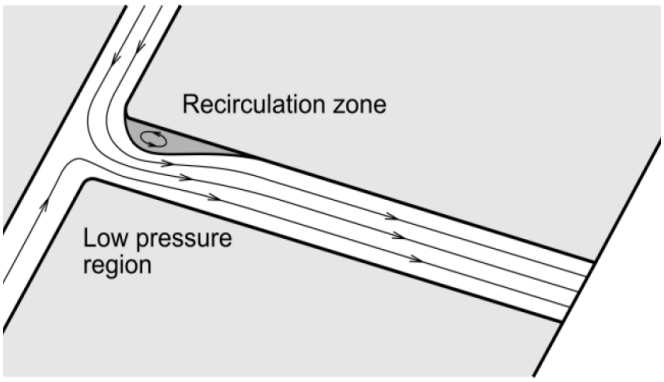

Figure 2.7: *A simplified sketch of cavitation and vena contracta occuring in the nozzle hole [27].*

Several factors can affect the cavitation intensity, such as the pressure difference. In addition, according to equations 2.2, 2.3, 2.4, and 2.5, it is apparent that flow velocity,

density, and fuel properties play an essential role in the quality of the break-up. It is worth noting that nozzle geometry also contributes to creating turbulence and cavitation, which affects the break-up and atomization.

2.3.4 Nozzle geometry and spray characteristics

The nozzle design affects internal flow, which potentially influences the spray characteristics. As an example, Figure 2.8 schematically illustrates the flow pattern inside the sac volume and the orifice inlet. This figure shows that the flow pattern at the orifice inlet is not symmetrical and the flow would follow sharper rotation on one side than the other. It is expected that asymmetrical flow patterns generate more turbulence and cavitation, and consequently impact spray characteristics.

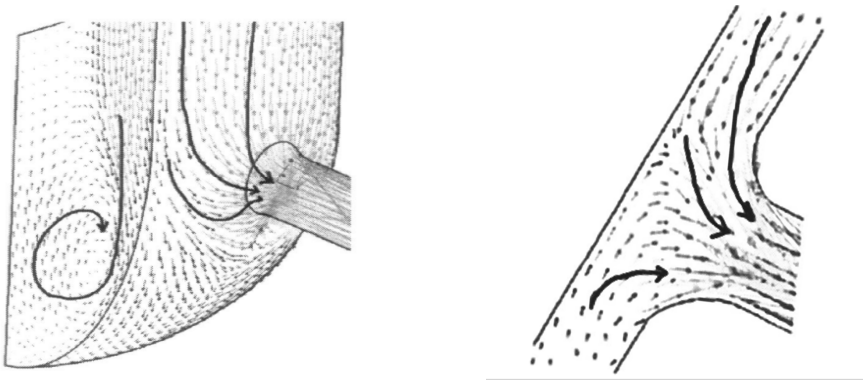

(a) (b)

Figure 2.8: *Schematic examples of flow streamlines a) inside a large sac volume, b) at the orifice entrance. (adapted from [36])*

The orifice outlet outlet area generally has a circular shape but can exist in other configurations such as elliptical, triangular, or rectangular, which come with their pros and cons. Elliptical orifices generate higher discharge coefficients and lower cavitation intensity compared to circular orifices. The axis-switching phenomenon is observed in rectangular [37], and elliptical [38], orifices, which enhances the break-up process and affects the flame-length [37, 39, 40].

Other nozzle geometry parameters that influence internal flow include the orifice angle, conicity, inlet edge radius, and length/diameter ratio.

Studies show that as the umbrella angle (α) increases, cavitation is more likely to occur, and its intensity will be higher [41, 42], resulting in a more dispersed spray [34, 43]. In addition, a larger umbrella angle decreases mass flow rate and momentum flux due to the higher deflection in the streamline, resulting in more turbulence and higher vortices [44, 45]. Regarding the conicity levels, orifices exist in 3 configurations, cylindrical, convergent,

and divergent, characterized by k-factor (equation 2.1). Reducing the k-factor from positive (convergent) to negative values (divergent), increases cavitation and turbulence leading to significant spray cone angle [33, 46, 47]. A divergent conical structure will dramatically accelerate the flow to initiate cavitation and promote the occurrence of hydraulic flips [48] which results in a slightly delayed spray tip penetration [46, 47, 49] while higher k-factors result in larger spray tip penetration and smaller spray cone angles [49]. Accordingly, the Convergent hole nozzle exhibits higher discharge coefficients and flow rates while cylindrical and divergent nozzles show decreased discharge coefficients with cavitation onset and hydraulic flip [33]. They even produce larger vapor cone angles than the convergent nozzles, indicating better air-fuel mixing and lower soot emissions [10].

A convergent orifice (k-factor>0) provides a higher mass flow rate and discharge coefficient with less cavitation intensity compared to the divergent orifice (k-factor < 0) [50]. In addition, a large k-factor generates a smaller spray cone angle while accelerating spray tip penetration evolution [49].

The orifice inlet radius can be increased by hydrogrinding, which is an effective way to reduce cavitation intensity and occurrence. This process will increase the discharge coefficient, attributed to the increased effective nozzle area [12]. In addition, larger inlet radii tend to produce higher initial velocities and more turbulence compared to sharp inlets [51], while producing larger droplets and longer liquid core [12]. Hydrogrinding and increasing the k-factor both slow down primary break-up, produce larger droplets, and increase penetration. However, hydrogrinding results in a higher discharge coefficient compared to an increased k-factor [8].

Length-to-diameter ratio (L/D) is another geometrical feature of the orifice that can affect spray morphology. Nozzles with smaller L/D ratios exhibit higher cavitation densities, larger spray cone angles, more turbulence, and higher spray velocity [34, 26]. However, smaller orifice diameters and longer orifice lengths improve spray atomization, which results in smaller SMD and improved combustion performance [11].

2.3.4.1 Hole-to-hole variation

The number of nozzle orifices affects both the fuel distribution and the behavior of individual spray. For example, nozzle sac pressure re-builds faster in the single-hole case than a multi-hole nozzle [52]. There is a higher fluctuation in sac pressure for the multi-hole nozzle, attributed mainly to eccentric needle motion that generates hole-to-hole spray variations [53]. In addition, a larger total orifice flow area makes the multi-hole nozzle more sensitive to rail pressure changes [54]. Multi-hole nozzles generally produce higher turbulence and radial velocity vectors due to complex internal flow, leading to wider spray dispersion angles [54, 55, 56]. The higher cone angle is beneficial regarding better air entrainment, enhancing the air-fuel mixing, especially in transient phases [57]. Nozzle geometry and ambient density are the main parameters that affect spray cone

angle [47, 58] while injection pressure has a negligible effect on this matter [59, 60]. Often the spray angle is inversely related to the spray penetration length; i.e., a wider spray has a shorter penetration length at the same injection rate [58, 47].

The sac volume functions as a buffer, producing a more consistent flow distribution among the spray holes. It also produces a smoother transition and a more streamlined entrance into the holes. However, at the end of the injection, still, a considerable amount of fuel is still trapped in the sac volume and may exit the nozzle orifice with low velocity. This results in the formation of more soot and unburnt hydrocarbons, especially for cases with large sac volumes [36]. In some cases, the holes are created at the needle seat instead of the sac volume, called VCO. This can reduce soot formation at the end of the injection but it creates significant hole-to-hole variations.

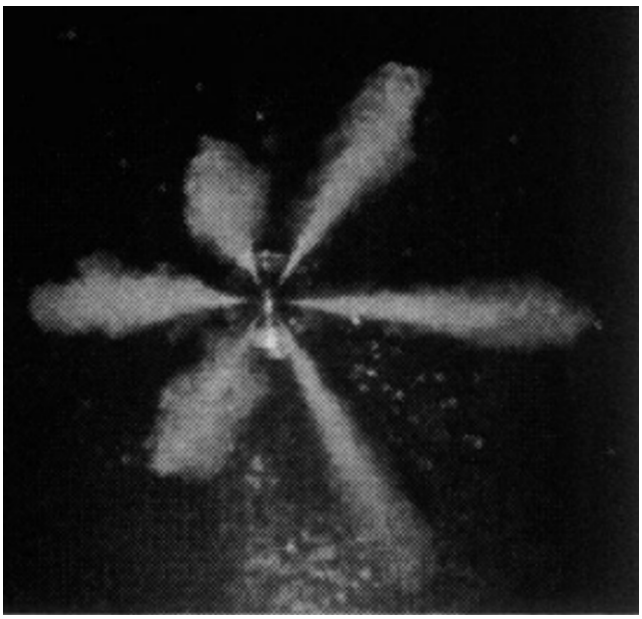

Figure 2.9: *Hole-to-hole variation and unequal sprays*

Hole-to-hole variations may have other reasons as well, which are divided into three main categories:

1. Geometrical differences in orifices are the main reason, which can be the result of poor manufacturing quality, erosive damage, or variable amounts of coke deposition.
2. Installing the injector with an inclination angle generates orifices with different angles to the horizontal plane. Thus, the flow path for those orifices will differ, resulting in hole-to-hole spray variations.
3. The eccentric needle motion affects the internal flow and induces oscillations in spray velocity. However, studies show that for a multi-hole injector, the oscillation phase, frequency, and amplitude of spray axial velocity are similar for all holes regardless of the number of holes. In addition, the needle lift also influences the internal flow and hole-to-hole spray variations. The needle seat area is smaller

than the hole area for small lift; Therefore, a slight needle mismatch contributes to the misdistribution of the needle seat area (incoming flow area) and internal flow. However, as the needle lift, and thus, the needle seat area increases, this effect becomes more negligible. The internal flow area determines the flow state and spray characteristics behavior. The internal flow area determines the flow state and thus injected spray characteristics; the moment the needle seat area is equal to the nozzle hole area is considered as the turning point from transient flow to quasi-steady state flow. Therefore, the effect of needle mismatch on hole-to-hole variations appears mainly during the opening and closing of the needle and not for the fully developed flow [61].

3 Methodology

This work investigates the effect of the nozzle geometry on the near-field spray kinematics. For this purpose, we measured the velocity of the near-field spray formed by nozzles with specific geometries under different injection pressures. The approach applies time-gated ballistic imaging to produce double-frame and time-resolved images with high resolution. With the aid of a normalized cross-correction algorithm, spatial structures on the spray interface are detected and tracked in each pair of images. The relative displacement of fluid structures of the spray over the time frame between two images is the approximate velocity of that area of the spray.

3.1 Nozzle geometries

This study contains an experimental investigation of four prototype nozzles and measurements of their spray kinematics. Figure 3.1 illustrates schematics of these nozzles, and Table 3.1 provides nozzles specifications. As can be seen, the first two nozzles (SH1 and SH2) are both single-hole, and their orifice axis is aligned with the injector axis. Therefore, both orifices have a relatively symmetrical geometry along their axes (Figures 3.1(a) and 3.1(b)). The only differences between the two nozzles are the orifice diameter and k-factor. Although the third nozzle (OA) is also a single-hole nozzle, its orifice axis is located parallel to the injector at a short distance from the centerline. Therefore, it has an asymmetric geometry at the inlet and outlet of the orifice (Figure 3.1(c)). Unlike the other nozzles, the last one (TH) has two orifices with an umbrella angle of 146°(Figure 3.1(d)). Regarding geometrical aspects, this nozzle is very similar to the nozzles currently used in production but is more practical to study due to the simplified geometry with fewer holes. This nozzle allows investigating hole-to-hole spray variations while oblique orifices also create asymmetrical geometry.

Table 3.1: Nozzles specifications

Nozzle	$SH1$	$SH2$	OA	TH
Number of orifices	1	1	1	2
Nominal outlet diameter [μm]	140	180	220	200
k-factor	0	2	1.4	2
Hydro-grinding level [%]	30	30	15	15
Spray target angle [°]	90	90	90	17

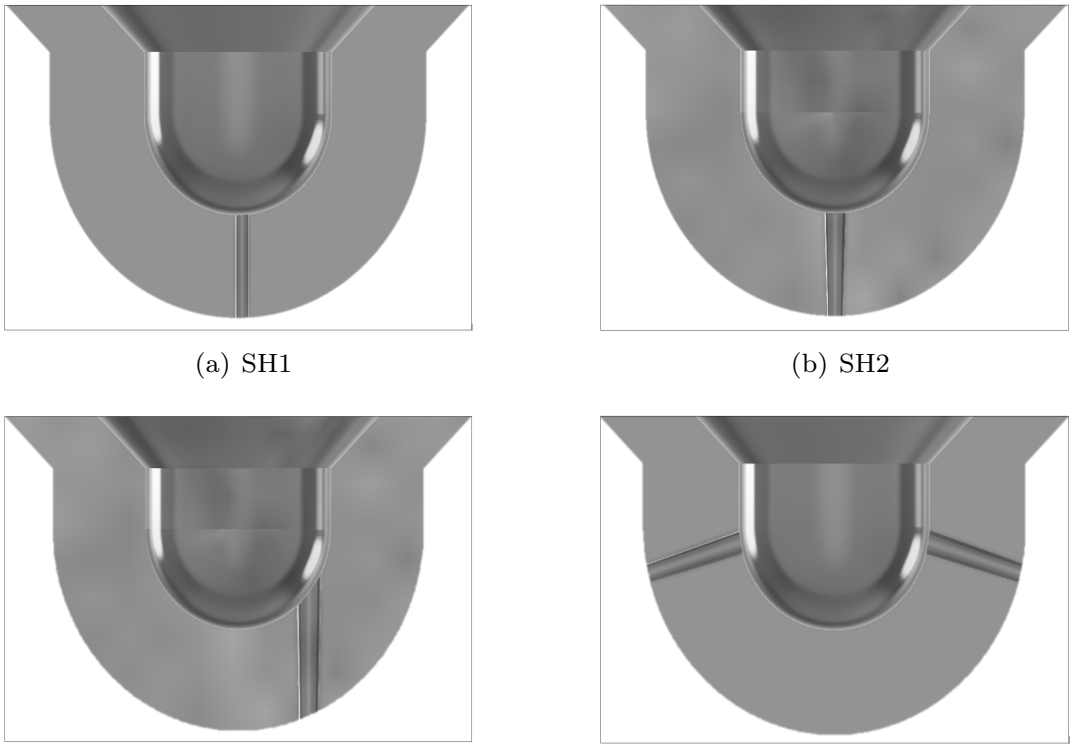

(a) SH1 (b) SH2

(c) OA (d) TH

Figure 3.1: *Cross-section view of the nozzle geometries.*

3.1.1 Injector mount

To accommodate XPI injectors within the spatial constraints of the spray chamber, a custom injector holder was designed, as shown in Figure 3.2. Given the side-fed configuration of the XPI injectors and the limited space within the housing port, the injector is installed at a diagonal angle of 21°. However, this setup prompts considerations regarding the potential impact of gravity on fuel flow dynamics within the nozzle and orifices.

Notably, for the two-hole injector, one orifice faces downward with a 4° inclination to the vertical axis, while the other orifice points upward with a 38° angle. While this design effectively meets the research requirements, it is imperative to acknowledge and address the minor gravitational effects on the fuel flow dynamics.

3.2 Velocity measurement

In the study of fluid dynamics, choosing the right tools to measure spray velocity is crucial. Different techniques offer various insights, each having its strengths and limitations.

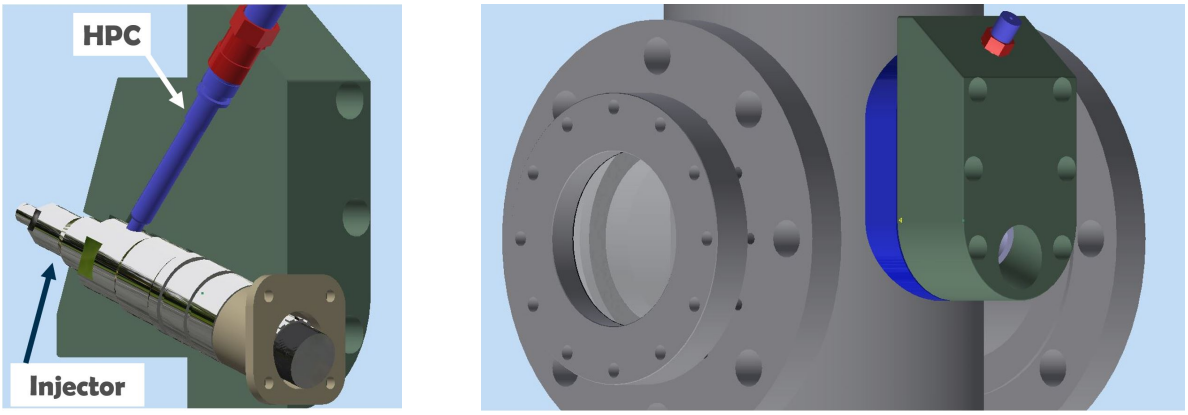

(a) Injector assembly

(b) The assembly mounted on the chamber

Figure 3.2: *Injector mount that was specifically designed for the XPI injector and the spray chamber*

Common methods include Phase Doppler Anemometry [62], Particle Image Velocimetry [63], Laser Doppler Velocimetry [64], and Image Correlation Technique [65], which are briefly explained below.

- **Phase Doppler Anemometry (PDA):** PDA is a method used to understand the size and speed of particles or droplets in a fluid flow. It involves multiple laser beams intersecting in a measurement area, where detectors capture scattered light from particles. As particles move through the lasers, they create interference patterns, and by analyzing the differences in signals received by detectors, it is possible to determine their velocity. PDA provides detailed information about particle size and velocity but is relatively more complex and costly compared to some other methods. It works best within a specific droplet size range, and its accuracy may decrease for very small or large particles. However, it may face challenges in optically dense flows and the near-field spray.

- **Laser Doppler Velocimetry (LDV):** LDV gauges fluid motion by leveraging the Doppler shift in laser light scattered by particles or molecules in the fluid. A coherent light beam splits into a measurement beam directed into the flow and a reference beam. These beams intersect within the measurement area, and particles scatter light, creating an interference pattern. The Doppler shift in the scattered light's frequency is detected, revealing the velocity of particles and, consequently, the fluid along the laser beams. LDV requires a clear optical path and is sensitive to alignment, necessitating careful calibration. It may not be suitable for high-speed flows, and variations in particle concentration can impact measurements.

- **Particle Image Velocimetry (PIV):** This method relies on seeding the flow with tracer particles, such as small droplets or reflective particles, and illuminating them with a laser sheet. The motion of these particles is captured by a high-speed camera, and the displacement between successive frames is analyzed to calculate

the flow velocity. To ensure accurate results, the particles used in PIV should possess specific properties, including small size, low inertia, and a rapid response to the flow. Common seeding materials encompass oil droplets, smoke particles, or specially designed tracer particles. The velocity vector field is determined by analyzing particle displacement between frames using cross-correlation algorithms. Although this method has proved to be highly accurate, it is not practical for near-field spray application due to high flow density. In this spray region, either no particle is formed, or they are too small to be detected. In other words, this method is applicable for more dilute spray regions.

- **Image Correlation Velocimetry (ICV):** ICV is a method that analyzes pairs of images captured in a fluid flow using image correlation techniques. These techniques track the displacement of features or particles between successive frames to calculate the velocity field. ICV is specifically designed for unseeded flows and employs correlation techniques similar to Particle Image Velocimetry (PIV). The process involves matching algorithms for estimating velocity, whether by labeling the flow with trackable features, matching the motion of naturally existing features within the flow, or predictively morphing and validating the scalar field. While velocity outputs from ICV methods can provide high-quality results, it is crucial to rigorously evaluate them as correlation errors with unseeded images may be significantly larger than in PIV. To achieve optimal results, sharp, highly resolved structures in both time and space are essential. These requirements can be fulfilled using time-gated ballistic imaging for image acquisition. Sedarsky et al. [66] have proven this method to obtain near-field spray velocity vectors.

  In the current application, velocity measurements are constrained to the spray periphery due to the availability of traceable features exclusively at this region. Consequently, this method is unable to offer insights into the liquid core velocity at this stage. However, by employing the same measurement procedure on various spatial planes at different view angles (rotated around the orifice axis), it becomes feasible to comprehend the overall spray behavior and its velocity profile. A similar approach has been validated by Sedarsky et al., confirming the effectiveness of this method in understanding spray dynamics [67].

3.3 Optical setup

Time-gated ballistic imaging is a line-of-sight imaging method that was initially used for medical purposes, but this method was implemented to study sprays as well. The principles of this method have been described in detail by Linne et al. [68]. In short, the photons passing through the spray without colliding with the spray or with very little interaction have a higher speed than the others, and they reach the detector in a shorter time. In addition, a so-called optical shutter rejects the multi-scattered photons and allows the other photons to reach the camera, resulting in high-resolution spray images.

This optical shutter is called the OKE gate and consists of two cross-polarizers and a birefringence medium. When a switching pulse activates birefringence in that medium, the polarization of transmitted photons is rotated by 90°, and photons can go through the second polarizer. However, the gate activation period is approximately 2 ps; therefore, any photon that reaches the medium after that period cannot find a way through the second polarizer. Consequently, this imaging method can eliminate multiple scattering noises, reduce image blurring, and create sharp images with high resolution.

Ballistic images are two-dimensional representations of three-dimensional structures, and they can show large features that refract light instead of scattering small droplets. However, The liquid volume fraction of these structures might be smaller than 100% because they could consist of distributed sheets with entrained gas [69]. Nevertheless, the images appear monolithic even if the interior consists of a mixture. The utility of BI is to reveal the left and right-hand edges of liquid structures buried inside drop clouds. As Falgout et al. [70] have shown earlier, The spray structures in ballistic images are distinct and provide a well-defined interface. In contrast, these edges are diffuse in shadow images with structures that indicate a dropping cloud (Figure 3.4). Therefore, there is no clear, defined gas/liquid interface, as seen in the BI of the same jet.

The optical arrangement for the imaging system is according to the "collinear ballistic imaging" [71]. In this configuration, the frequency of the imaging beam is different from the switching pulse, and both of them reach the OKE gate in a co-linear configuration. The optical setup for this work is based on collinear ballistic imaging with two lenses (4

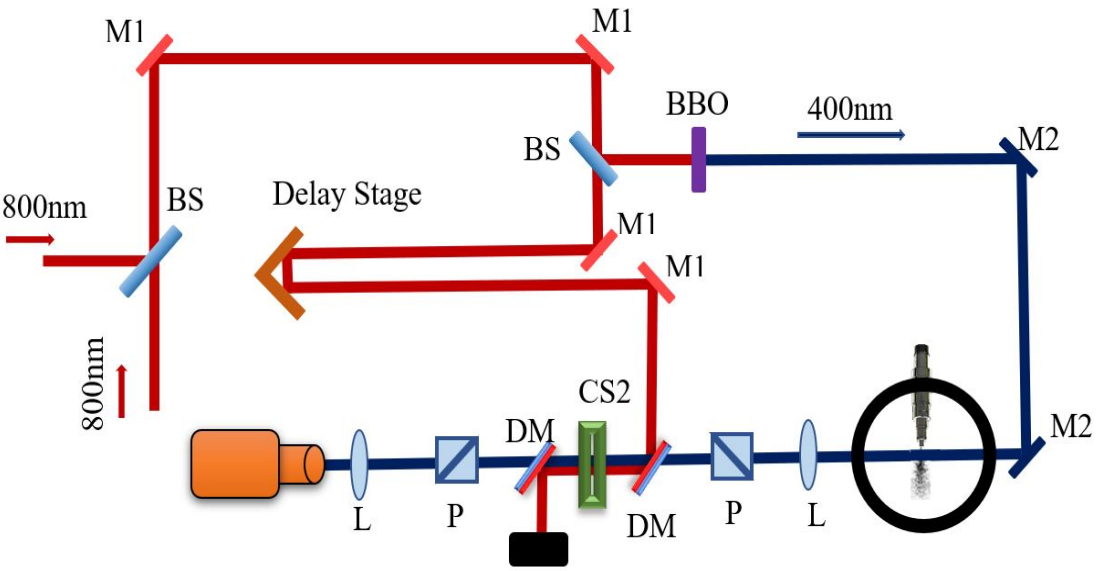

Figure 3.3: *A schematic view of image acquisition system configuration. M1: 800 nm mirror, M2: 400 nm mirror, BS: beam splitter, P: polarizer, L: lens, DM: dichroich mirror.*

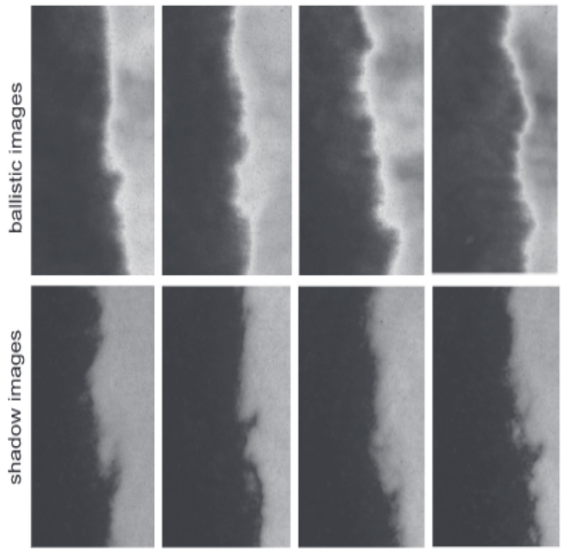

Figure 3.4: *Comparison between ballistic images (top) and shadow images (bottom) [70]. It shows that ballistic images provide a more clear liquid/gas interface than the shadow images of the same nozzle and fuel.*

focal points) as depicted in Figure 3.3. In this setup, two 100 fs laser pulses with the wavelength of 800 nm are generated with an adjustable time difference. First, both beams are aligned together using a beam-splitter. Then, a beam-splitter divides each beam into two portions; the part containing higher energy works as the switching beam after being transmitted through the delay stage. Finally, the other portion will be transmitted through the spray and camera to construct the spray image. A double-frame ICCD camera records the image signals.

This configuration allows recording only one image per laser pulse for each injection event but that provides more information about the spray structure and preserves spray interface in high resolution. Therefore, recording the entire injection process is unattainable, as is usually done by high-speed video cameras. Hence, the approach to this problem is to perform statistical velocity measurements. In this approach, image acquisition was performed for discrete-time instants from the start of injection to 50 μs. It is recommended to take between 150 and 200 images for each step to have a sufficient statistical sample to measure the statistical velocity.

3.4 Design of experiments

The experiments were performed at the spray laboratory at Chalmers University of Technology. In these experiments, fuel injections occur in a constant volume chamber operating at atmospheric conditions. A high-pressure pump supplies fuel to the injector over a range of pressures up to 1600 bar. For this work, three levels of low, medium, and

high injection pressures were considered. Other experimental conditions are shown in Table 3.2.

Table 3.2: Experimental conditions

Parameter	**Value**	**Unit**
Rail pressure	800, 1200, 1600	bar
Back pressure	atm	-
Ambient temperature	294	K
Injection duration	2	ms
Image pairs time difference	560	ns

Here, the Start Of Injection (SOI) refers to the moment that the spray is on the verge of leaving the nozzle, and other time instants are defined based on this moment. To determine the SOI, a set of images was taken just before the estimated SOI until the flow became visible. We set the time increment between images to 1 μs. Assuming that the velocity of the spray at the beginning of injection is linear, measuring the reverse displacement of the spray to the penetration length of zero yields the time instant of hydraulic SOI.

3.5 Data processing

3.5.1 Experimental data

Image processing procedures that are applied to all images include background removal and normalizing. In addition, a bilateral filter is applied to minimize the noise coming from the non-uniformity of the laser beams, as well as the residuals from previous injections. By implementing a cross-correlation algorithm, displacement vectors can be extracted at the spray periphery. This algorithm is described in detail in [66] and [72]. As a short explanation, we define a set of windows called "template" and "search field" and adjust their size according to the application. Then, the Sobel edge detection method catches the spray periphery, and several points are distributed on the edge of the spray as "target points". Each target point is the origin of a template window. The texture and intensity information inside the template should match with a similar window in the search field area of the second image. The position difference of those template windows yields a 2D displacement vector for each target point. Finally, each vector should be validated or rejected based on the input parameters, such as allowable displacement in either direction or cross-correlation coefficient.

It is worth mentioning that all images taken at any time instant indicate the diversity of the spray profiles. Therefore, we can construct an overall spray profile by calculating the average of all the images at the respective time step. Then, by averaging all available

velocity data in the vicinity of any point on the overall spray profile, the average velocity for each point is calculated as the local velocity.

In addition to sampling sprays based on the start of injection (SOI) time, an alternative method involves sorting sprays according to their penetration length. This is crucial because sprays triggered at the same time instance exhibit deviations in penetration length. These variations may stem from different sources, such as eccentric needle motion, electromagnetic interference causing off-timing, and rail pressure fluctuations. To address this, a computer vision code was developed to sort images based on the penetration lengths of each spray. This approach proves to yield more consistent velocity information compared to SOI-based sorting. It's important to note that this method is applicable only when the entire spray is visible, limited by a 4 mm field of view. This approach was quite beneficial when validating the simulation model.

3.5.2 Simulation data

A validated model not only provides insights into intricate internal flows but also serves as a cost-effective and time-saving tool to explore the effects of various parameters on the flow. Additionally, it contributes to the optimization of nozzle geometry and offers valuable inputs for other simulations, such as far-field flow simulations.

General model description

Within the framework of this research, a simulation model tailored for the near-field of the spray was developed using the Scania-Cummins collaboration. The simulation was conducted utilizing AVL Fire, a powerful computational fluid dynamics (CFD) software. The geometric configuration of the model was derived from X-ray Computed Tomography (CT) data, ensuring a realistic representation. The model adopts the Eulerian approach, employing a multi-fluid approach to accurately capture non-equilibrium conditions among different phases within the system. This approach allows each phase to exhibit distinct temperature, pressure, and velocity profiles. One of the primary objectives of this research is the processing of simulation data and the subsequent validation process. The challenges inherent in this process are noteworthy and merit detailed discussion in the thesis. Addressing these challenges is pivotal to ensuring the reliability and accuracy of the simulation results.

Data selection

The simulation allows the study of various attributes for each phase, presenting challenges in data selection. The data can be discretized based on liquid volume fractions or spatial coordinates, with added complexity when considering the injection time instance. To establish a reliable data selection procedure, understanding the experimentally measured attributes is crucial.

Ballistic imaging provides spatial data about the liquid core and air-entrainment/evaporation

interface. Optimal selection involves choosing cells with minimal liquid volume fractions, considering the spray velocity profile. Although no specific threshold is prescribed, averaging volume fractions may yield a more accurate velocity distribution profile. In addition, the optical depth of field (100 μm) suggests limiting simulation data to the coordinates within $\pm 50 \mu m$ distance from the observation plane.

Experimentally collected data comprises different sprays in terms of shape and penetration length. Matching identical sprays is challenging, prompting the swapping of spray timings in the simulation within corresponding penetration lengths from the experiment, which simulates similar conditions.

Figure 3.5 compares different data selection approaches with the experimental data at various distances from the nozzle. Accordingly, the optimum data selection consists of considering liquid volume fractions below 10%, within range of the optical depth of field, and $\pm 5 \mu s$ of injection time swap, establishing the approach to align simulation data with experimental conditions.

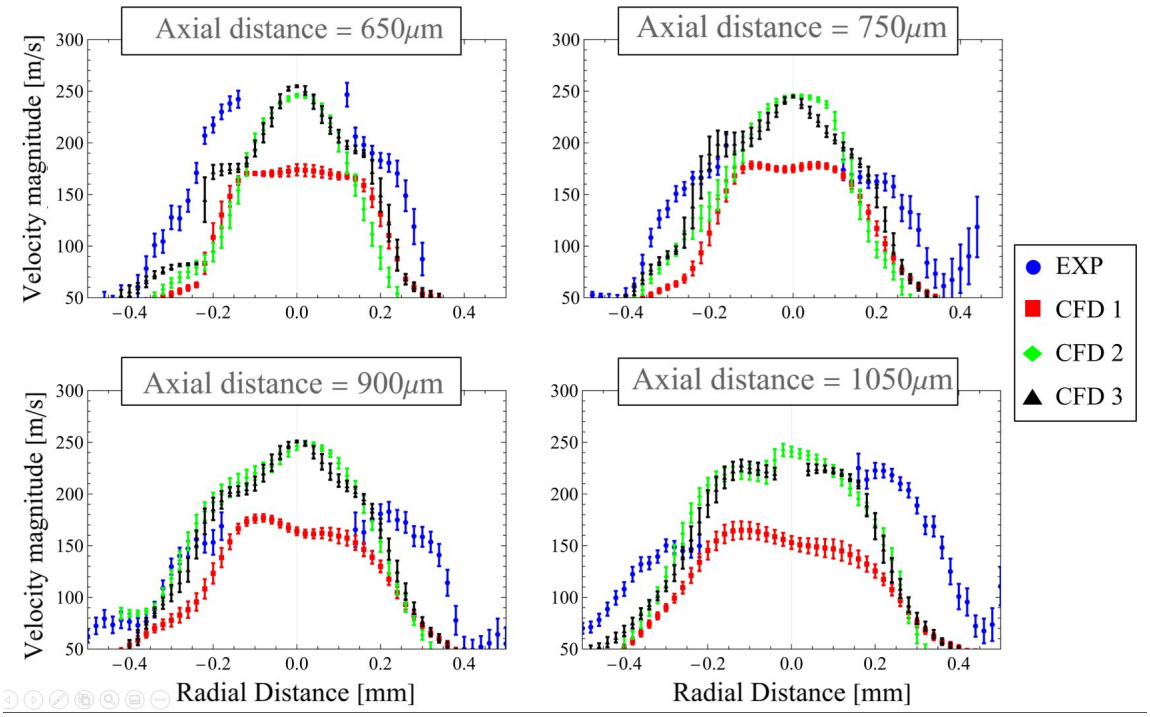

Figure 3.5: *Data selection approaches for comparing CFD vs experimental data. In this figure CFD1 includes all volume fractions below 10%, CFD2 represents velocity data of all volume fractions limited to $\pm 50 \mu m$ from the observation plane, and CFD3 belongs to volume fractions below 10% limited limited to $\pm 50 \mu m$ from the observation plane.*

4 Contribution to the field

This section provides an overview of the findings detailed in the appended articles.

4.1 Summary of appended publications

4.1.1 Publication A

Near-field spray velocity and development in single-hole diesel injector

This publication represents the first attempt in this research to employ collinear time-gated ballistic imaging and normalized cross-correlation for measuring the near-field spray velocity. The study focuses on single-hole on-axis nozzles, namely SH1 and SH2, which vary in orifice diameter and conicity. The primary objective is to assess and compare the effects of outlet diameter and k-factor on the spray near-field spray dynamics. These investigations are crucial for establishing baseline conditions and guiding future research directions.

The experimental phase, conducted over the early transient period (20–50 μs) after the hydraulic start of injection, provides an understanding of the dynamics and morphology of the spray. In particular, the research covers a spectrum of conditions by varying the rail pressures at 800, 1200, and 1600 bar. The findings offer compelling insights into the relationship between injection pressure and spray characteristics. As injection pressure increases, the spray velocity magnitude increases, with a notable emphasis on radial components. Beyond a specific pressure threshold, the dominance of radial velocity results in a wider spray cone, while axial penetration shows marginal improvement. The observed phenomena are intriguingly linked to the potential occurrence of cavitation, particularly at higher injection pressures.

Another aspect of the study pertains to the SH2 nozzle, which exhibits a subtle deviation in the spray axis. This deviation appears to be intricately connected to the velocity balance at the spray's periphery. Remarkably, the nozzle with a smaller k-factor and diameter does not exhibit any evidence of spray deviation in the studied region.

Further examination of the region proximate to the nozzle tip (0–0.5 mm) reveals consistently lower velocity magnitudes over this region. This phenomenon is attributed to the non-slip conditions at the orifice exit. The non-slip condition means that the fluid adheres to the solid surface at their interface. In this case, the fluid sticks to the orifice wall, moving at the same speed as the wall itself which is near zero.

The investigation also delves into the correlation between pressure and Nozzle Opening Delay (NOD), revealing a notable reduction with increasing pressure. Simultaneously,

the transient phase in spray development demonstrates a tendency to become shorter in duration as pressure level is increased.

In a broader context, the study highlights that the nozzle with a smaller hole diameter consistently generates sprays characterized by higher overall velocities. Notably, the difference in nozzle geometry emerges as the pivotal factor shaping the spray, with the impact of injection pressure varying between nozzles. Specifically, as Figure 4.1 clearly illustrates, the nozzle with a more cylindrical shape exhibits a significant widening effect at higher injection pressures. In contrast, this effect remains negligible for the convergent nozzle.

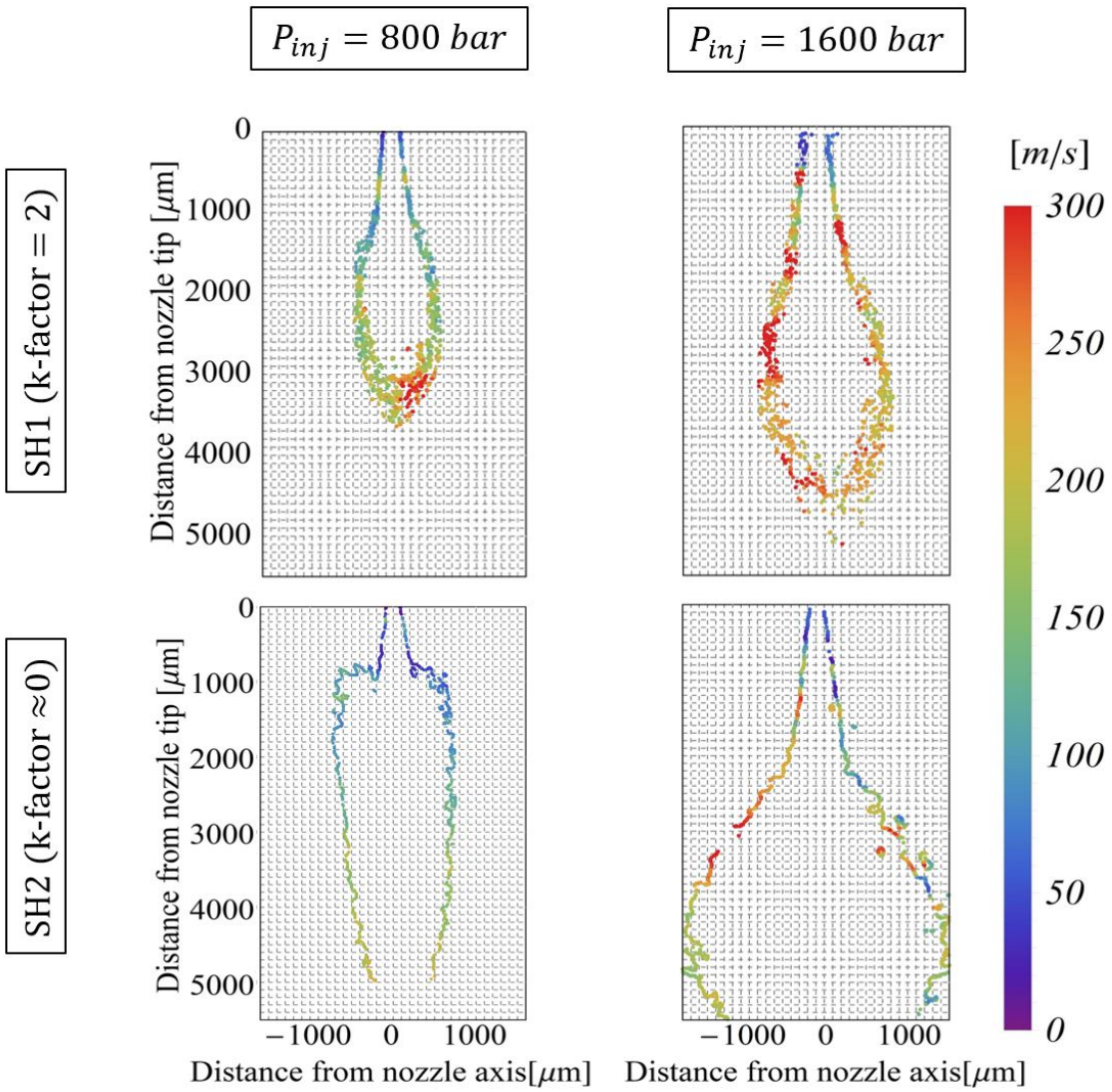

Figure 4.1: *Near-field spray velocity distributions for two nozzles and injection pressures at 40 μs after SOI. This figure clearly shows how a nozzle with a smaller k-factore is influenced by a higher injection pressure.*

Author Contributions:

M. Nikouei: Experimental setup, conducted experiments, data analysis, writing the manuscript.

D. Sedarsky Method, supervision, velocimetry code development.

4.1.2 Publication B

Effect of asymmetrical orifice inlet geometry on spray kinematics and development

This article represents a continuation of Publication A, with a distinct focus on the off-axis and two-hole nozzles. In contrast to the prior publication, this study concentrates on the single-hole off-axis nozzle, which creates an asymmetrical geometry at the inlet and outlet of the orifice, potentially leading to asymmetrical turbulence and increased potential for cavitation. The two-hole nozzle was chosen for its relevance to in-production multi-hole nozzles. This nozzle features only two holes precisely positioned on opposite sides, making it ideal for spray diagnostic applications.

Employing the same methodology as Publication A for image acquisition and data processing, this study measured and collected velocity information for 45 sprays across three orifices, three injection pressures, and five-time instants. Over 150 image pairs were processed for each case to statistically investigate the effect of asymmetrical orifice inlet on spray kinematics.

Similar to Publication A, observations revealed a near-zero velocity at the spray periphery just ($\leq 20\mu s$) after the hydraulic start of injection. This initial low velocity is attributed to residual fuel and air in the sac volume from the prior injection, which shows slight resistance against the fresh incoming flow. As the needle rises, momentum exchange and mixing lead to a brief acceleration, followed by velocity reduction downstream, where the spray's momentum energy dissipates.

Analyzing the radial velocity components of the off-axis spray revealed a notable motion during a specific injection period, where the trailing edge of the spray plum exhibited the opposite velocity direction to the leading edge expansion direction (Figure 4.2).

The study highlighted that asymmetrical inlet geometry, particularly in the off-axis nozzle, led to a deviation of the average spray axis towards the side with a sharper orifice inlet edge, impacting spray targeting. Velocity distribution also became asymmetrical on opposite sides of the spray with increasing injection pressure.

Moreover, the injection pressure influenced nozzle opening delay, needle acceleration, spray tip acceleration, and evolution. Higher injection pressure reduced the time for spray

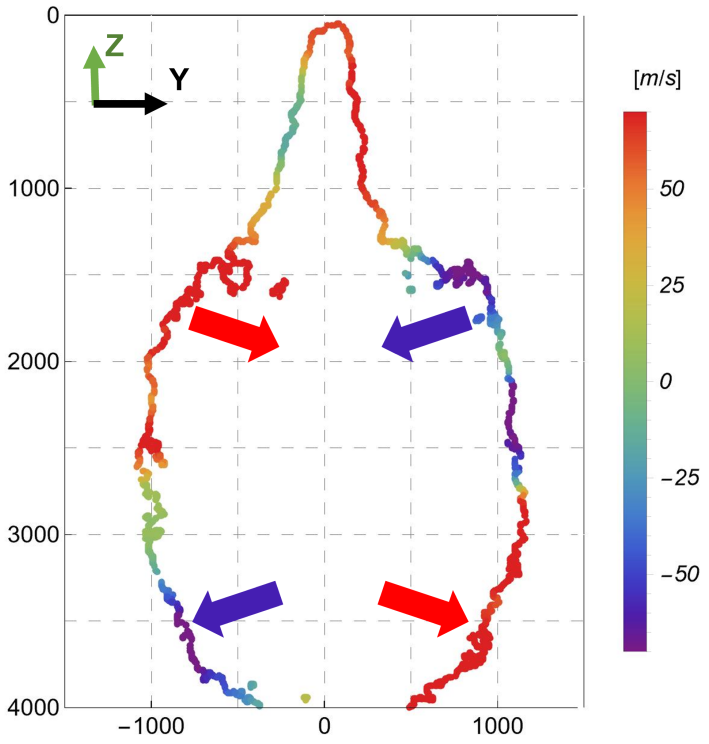

Figure 4.2: *Average radial velocity (in Y direction) of the spray generated by the off-axis nozzle at 30 µs after SOI under 1600 bar. This figure shows that the leading edge and the trailing edge of each side have opposite directions.*

evolution by increasing flow velocity and acceleration, shortening the transient phase by accelerating the needle movement. However, the injection pressure did not influence the overall spray profile.

In examining the two-hole nozzle, the study anticipated low sac pressure variation due to its fewer holes compared to conventional injectors. Consequently, there were no significant variations observed in both holes, producing unique sprays in terms of shape, yet nearly identical penetration rates. A wider spray with higher radial velocities from one orifice raised questions about minor geometrical differences and injector orientation. The diagonal mounting of the injector body induced a severe change in the flow direction for one orifice, resulting in increased turbulence intensity and spray expansion.

Author Contributions:

M. Nikouei: Experimental setup, conducted experiments, data analysis, writing the manuscript.

D. Sedarsky: Method, supervision, velocimetry code development, review the manuscript.

4.1.3 Publication C

Effects of asymmetrical orifice inlet on steady-state diesel spray and the near-field kinematics

Building on the insights from Publication B, this study, Publication C, takes a deeper dive into the quantitative analysis of spray characteristics and velocity distribution. The primary objective is to provide a more nuanced understanding of these factors by focusing on steady-state sprays occurring 600 microseconds after the hydraulic start of injection. The experimental approach mirrors the methodology employed in prior research works, ensuring consistency and comparability.

In this investigation, the spotlight is on sprays generated by both off-axis and two-hole nozzles, under the influence of varying injection pressures. The results offer a comprehensive view, encompassing spray profiles, velocity distribution in axial and radial directions, deviation angles, and near-field cone angles. Each case is examined the spray dynamics independently for each side and along the axial direction.

According to Figure 4.3, one notable finding underscores the predominant role of geometrical parameters in governing the spray profile. In addition, the injection pressure exhibited a comparatively limited impact. The off-axis nozzle stands out with a significant spray deviation, notably towards the side with a sharper orifice inlet. Importantly, the influence of injection pressure on spray deviation is evident, adding a dynamic element to the observed phenomena.

The radial velocity distribution reveals a distinctive behavior for the off-axis spray, where the radial velocity at the smoother side of the orifice approaches zero in many time instances and injection pressures. This implies that the axial velocity component is the primary component on this side.

Exploring fluctuations along the spray axis unveils their strength near the orifice outlet. The study also suggests a correlation between fluctuation frequency and amplitude with injection pressure, so that an increase in pressure leads to larger amplitudes and lower frequencies.

A key observation involves the calculated velocity ratio between the sides of the spray, attributed to the smooth edge and sharp edge of the orifice. On average, the velocity magnitude on the smoother side exceeds that on the sharper side by approximately 13%.

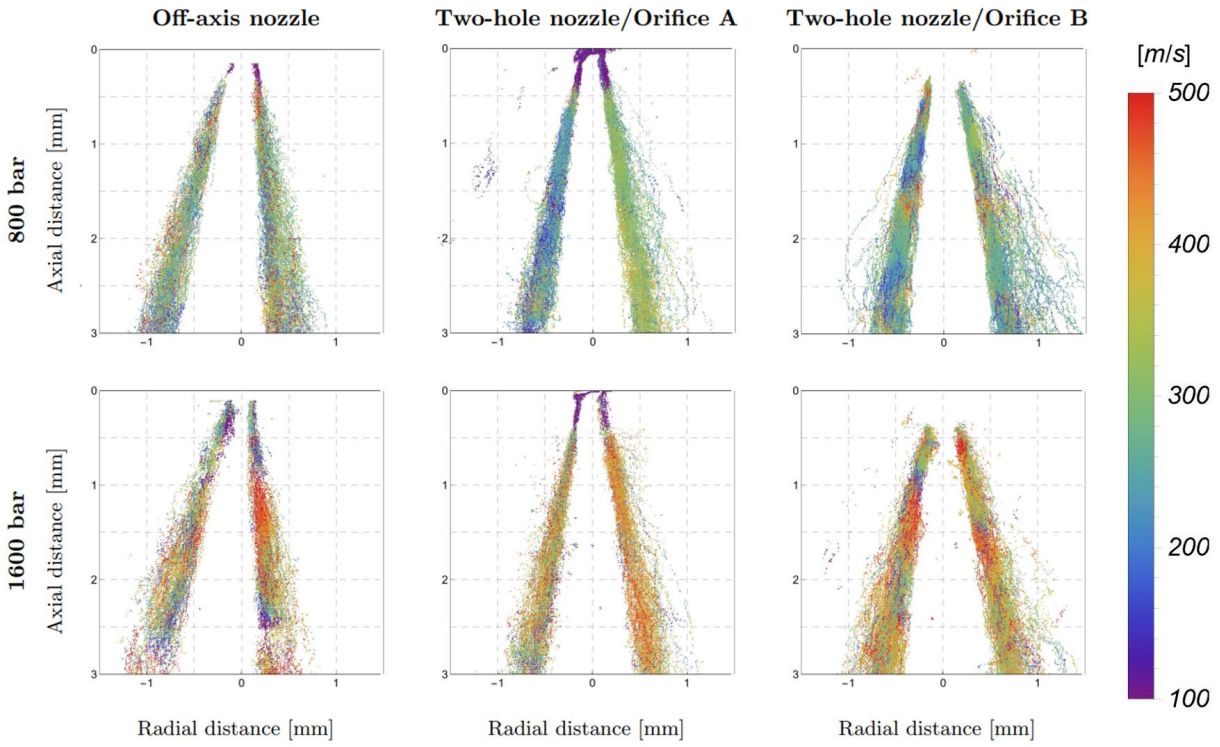

Figure 4.3: *Near-field spray profile and instantaneous velocity distribution for 3 orifices and two injection pressures at 600 µs after SOI.*

Author Contributions:

M. Nikouei: Experimental setup, conducted experiments, data analysis, writing the manuscript.

D. Sedarsky: Method, supervision, velocimetry tool development.

4.1.4 Publication D

Experimental Validation and Computational Insights into Near-Field Spray Dynamics and Internal Flow of Asymmetrical Off-axis Nozzle

This publication constitutes a pivotal phase in this research, building upon insights achieved from prior experimental work to validate a simulation model. In addition, this study aims to unravel the intricacies of internal flow within the off-axis nozzle, forging meaningful correlations with near-field spray characteristics and dynamics.

Executing simulations on the AVL Fire platform, we departed from conventional time-based spray approaches, opting for a penetration-based methodology. The procedure began by selecting sprays featuring a consistent 2.5 mm penetration length at 1600 bar as the baseline condition, serving as a foundational reference point for the refinement of the simulation model. Subsequent comparative analyses, encompassing variations in rail pressures and penetration lengths, were conducted to validate the model under diverse operating conditions.

In our simulation, we paid close attention to details like mesh intricacies and initial conditions. Specifically, we explored the sac's initial condition, varying the amount of liquid fuel present before injection—ranging from 5% (empty) to 50% (semi-full) and 95% (full). Notably, our analysis revealed that simulating an empty sac condition (5%) yielded results that closely aligned with experimental data, especially concerning axial velocities.

Recognizing uncertainties in experimental datasets and the process of CFD data selection, our findings underscored considerable agreement between experimental and simulated results, particularly concerning axial velocities. Following this validation phase, our exploration delved into the nuanced dynamics of internal nozzle flow, highlighting key aspects such as radial and circumferential velocity components. These outcomes showed an intricate interplay of opposing flows within the sac and orifice, with a specific emphasis on the influential role of the orifice's sharp inlet edge in shaping asymmetrical spray dynamics.

Beyond these internal flow dynamics, the CFD results revealed similar spray behaviors highlighted in previous research (Publication B). As shown in Figure 4.4, the periodic opposition in velocity directions between the leading and trailing edges of the spray at specific time intervals suggested the existence of a recurring circulation zone around the spray, showing a distinctive pattern that has been observed in experiments.

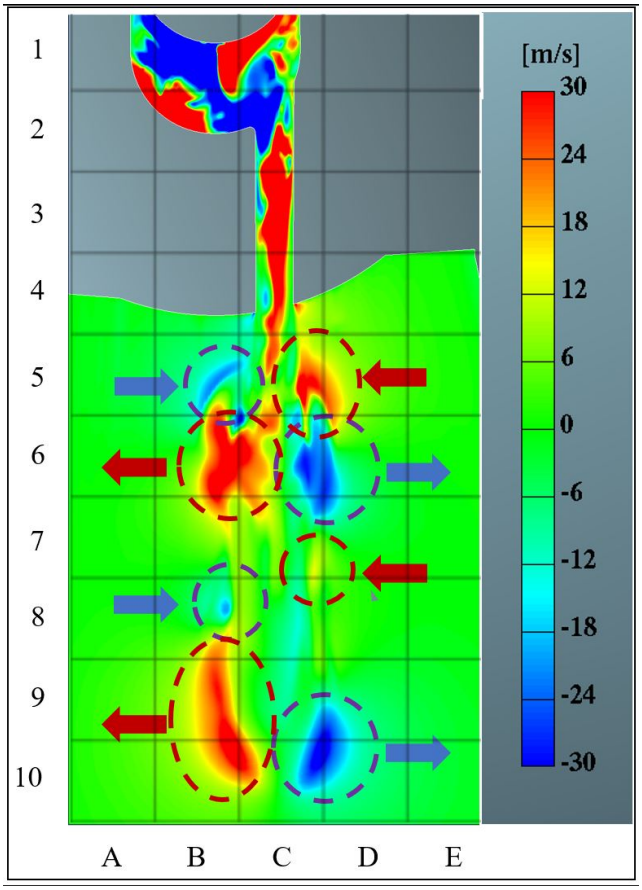

Figure 4.4: *Simulated opposite radial velocity directions between the leading and trailing edge of the spray*

Author Contributions:

M. Nikouei: Experimental setup, conducted experiments, CFD data processing, data analysis, writing the manuscript

D. Konstanzer: Simulation, writing the manuscript

N. Giramondi: Supervision, review the manuscript

D. Sedarsky: Supervision, velocimetry tool development

4.1.5 Publication E

Unveiling Spray Formation Dynamics During Early Transient Injection

This study serves as a complementary extension to Publications B and C, where the primary focus is on providing a more detailed and quantitative analysis of spray dynamics during the early transient phase of injection. Specifically, the research delves into the evolution of spray formation, adding a description of its characteristics under varying conditions. The investigation centers around three distinct nozzles, each subjected to different injection pressures, and employs a time-correlated approach to measure parameters such as the spreading angle and the spray axis angle. In addition, the study examines the local velocity of the spray, separately analyzing each side of the spray at every stage of the injection process.

The findings reveal that the spray axis exhibits noticeable deviations, which fluctuate not only during the transient phase but also in the quasi-steady state. These deviations, however, manifest differently depending on the nozzle type. For instance, in the case of an off-axis orifice, the deviations are more pronounced towards the cavitating side, whereas for a two-hole nozzle, the deviations are less significant and exhibit a more balanced distribution. This understanding of spray axis behavior highlights the sensitivity of bowl targeting with particular nozzle geometry.

Regarding the spreading angle, the spray initially expands, forming a mushroom-shaped fraction that peaks earlier under higher injection pressures. As the injection process transitions to a quasi-steady state, the near-field spreading angle stabilizes with only marginal changes across different injection pressures. However, a notable shift in the spreading angle occurs between 600 to 800 microseconds after the start of injection (SOI), suggesting a slight sweep in the spray pattern as the system reaches quasi-steady conditions.

The study also delves into the spray's velocity distribution along the spray axis. The axial velocity is found to vary significantly with the radial distance from the nozzle axis. In addition, reductions in velocity were observed with a higher distance from the nozzle tip, with a marked reduction beyond 2 mm, likely due to the drag resistance. This reduction points to the complex interactions between the spray and surrounding air, influencing the spray's momentum and overall behavior. In addition, the velocity distribution is influenced by factors such as needle lift and sac pressure dynamics, which contribute to a gradual increase in axial velocity over time. Notably, the non-slip condition near the nozzle leads to distinct velocity patterns within the first 0.2 mm, further complicating the velocity profile.

By reconstructing the spray geometry using the measured velocity vectors, the study uncovers insights into the relationship between spray dynamics and morphology. The reconstructed spray geometry often appears wider than observed, suggesting potential radial deceleration or the impact of spray dilution and evaporation. The presence of round

shapes and wrinkles within the spray adds another layer of complexity, likely affecting air entrainment and evaporation processes within the spray periphery.

Author Contributions:

M. Nikouei: Experimental setup, conducted experiments, data analysis, writing the manuscript.

D. Sedarsky: Method, supervision, velocimetry tool development, review the manuscript

5 Results and Discussion

This section presents a summary of the results obtained from this research. Figures 5.1 and 5.2 illustrate velocity profiles for the periphery of the near-field spray at discrete time instants after the start of injection. Each figure contains velocity information and the spray profile for five orifices at different injection pressures. The plots have been rotated and flipped horizontally for the off-axis (OA) and two-hole nozzle (TH) so that the side with a sharper orifice inlet edge lies on the negative side of the horizontal axis.

5.1 General trends

The results consist of the velocity data in the transient phase of the early injection. In this phase, the nozzle opening delay and the needle position also affect the flow velocity [43]. Figures 5.1 and 5.2 indicate that at a given time-instant, the spray profile and velocity of each nozzle vary with different injection pressures. Intriguingly, a comparable spray profile emerges at an earlier time step with increased injection pressure. For instance, focusing on the OA nozzle; the spray profile at 30 μs after the start of injection under 1600 *bar* resembles the spray at 800 *bar* and 40 μs. Nonetheless, it's essential to note that instantaneous local velocities are consistently higher at 1600 *bar*.

Shortly after leaving the nozzle, the fuel is accelerated, and a mushroom-shaped mass forms. The root of this mass might be related to the residual fuel trapped in the nozzle's sac volume from the previous injection [73]. This mass is pushed down by the pressure of the fluid coming out of the nozzle. Since the cross-sectional area of this mass is large, the drag force on the flow becomes more significant and it induces deceleration to the flow. Nevertheless, The incoming high-pressure fuel recovers the spray velocity. Finally, the velocity profile becomes more stable at the quasi-steady state (800 μs after SOI). Even during the steady state, variations in velocity magnitude along the spray axis are noticeable, both for the axial and radial components. However, as indicated by Figure 5.3, these fluctuations are not as pronounced as during the transient phase. Furthermore, it appears that these variations exhibit a significantly higher intensity in the case of the OA nozzle.

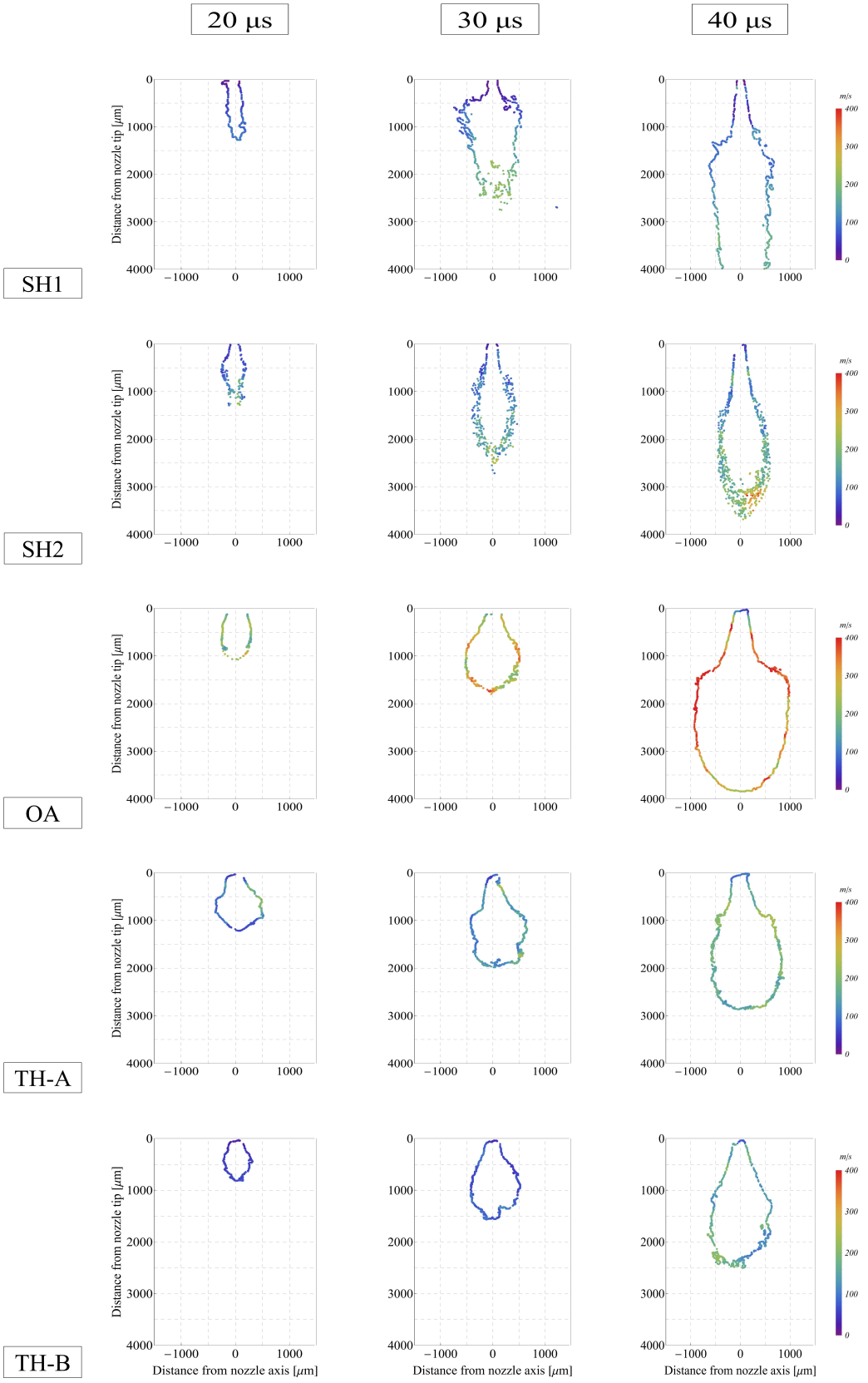

Figure 5.1: *Mean velocity magnitude for near-field sprays generated by five different orifices at 800 bar*

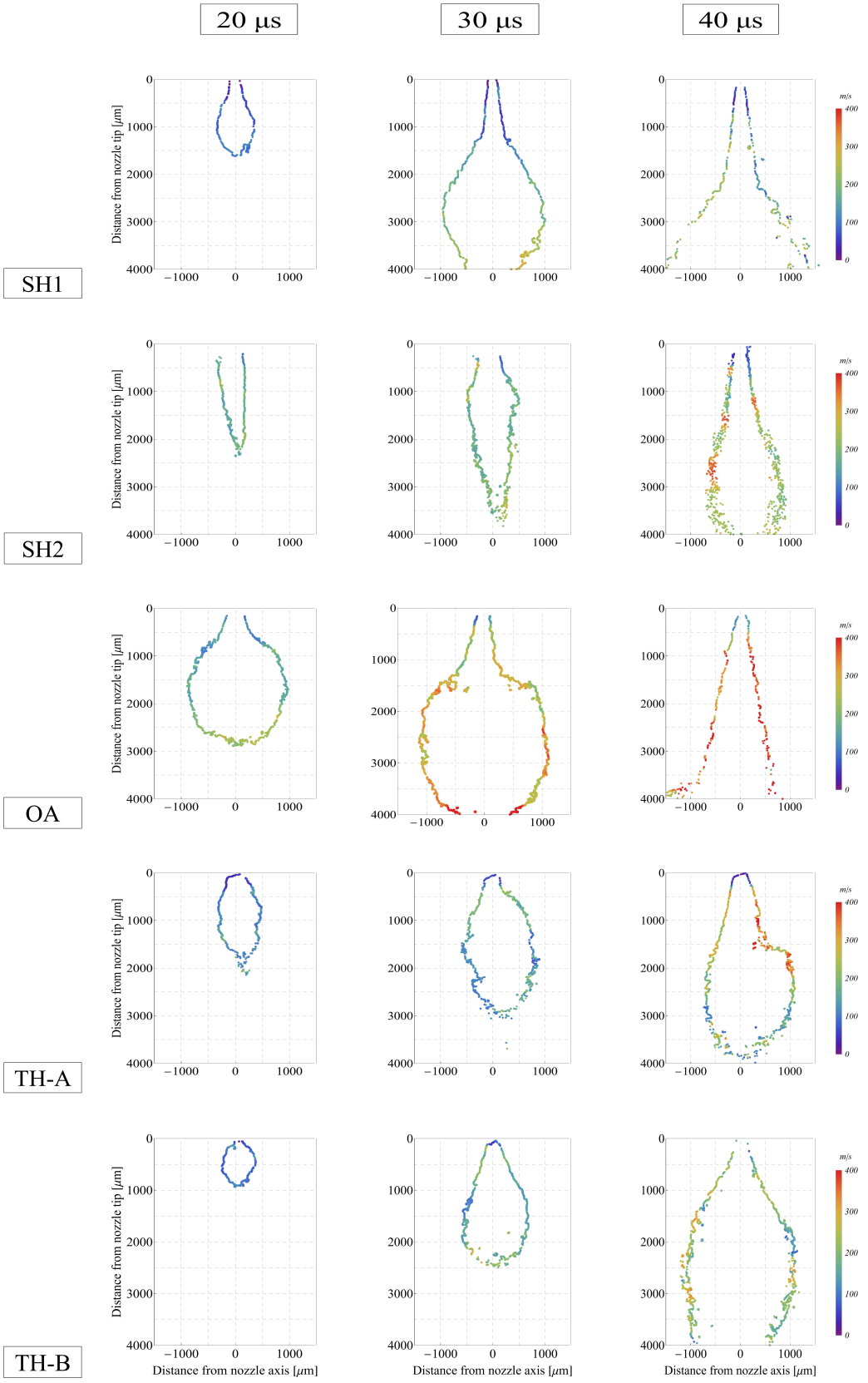

Figure 5.2: *Mean velocity magnitude for near-field sprays generated by five different orifices at 1600 bar*

5.1.1 Effect of nozzle geometry

Each row of Figures 5.1 and 5.2 consists of velocity profiles of a specific nozzle at different time steps. The comparison of these rows indicates that the overall spray velocities for both orifices of the two-hole nozzle are considerably lower than the off-axis nozzle. The difference in the total discharge cross-sectional area and the needle position could be the potential reason for that. Since the needle position is low at the beginning of the injection, the ratio between the incoming and outgoing flow rate in the sac volume is low. In addition, the presence of two orifices increases the discharge area and outgoing flow rate, which leads to an even lower sac inlet/outlet discharge rate, and causes a longer time for sac pressure recovery. When the needle reaches the highest lift position (at the quasi-steady state), the differences between overall spray velocities for the off-axis and the two-hole nozzles become smaller. This is in line with other studies [55], while Figure 4.3 also confirms this. This phenomenon is also evident when comparing the nozzles SH1 and SH2; this may contribute to higher spray penetration of the nozzle with a smaller orifice at corresponding time steps.

In the context of spray dynamics, it is important to note that while axial velocities vary among orifices, the disparities in their radial spray velocities are more substantial as shown in Figure 5.4. This discrepancy appears to contribute significantly to variations in spray profiles, influencing characteristics such as cone angle and deviation angle. Expanding the scope beyond spray dynamics, an in-depth examination in Publications C and E emphasizes that the overall spray profile is intricately linked to geometrical parameters. As depicted in Figures 4.3 and 5.5, there is a clear correlation between the spray deviation and these geometrical parameters.

5.1.2 Effect of injection pressure

Figures 5.1 and 5.2 show velocity profiles at 800 bar and 1600 bar respectively. According to these figures, injection pressure mainly influences the velocity and acceleration of the spray but it has a negligible effect on the overall spray profile, especially at steady-state. Nevertheless, increasing injection pressure beyond a critical value can also affect the prevailing spray profile in nozzle geometries that are more prone to cavitation. As discussed earlier, increasing the injection pressure boosts the spray deviation in asymmetric orifices, which is confirmed by the analysis provided by Figure 5.5. In addition, raising injection pressure impacts the cone angle marginally. In this regard, the near-field spray profile for the cylindrical nozzle seems very responsive to the pressure rise and becomes slightly wider. Hence, the influence of pressure on the spray profile can be regarded as a complementary factor. This implies that pressure exerts an impact on the spray characteristics when the nozzle exhibits pressure-sensitive attributes, such as a notably small inlet edge radius or a low k-factor. These features enhance the likelihood of cavitation, a phenomenon that, in turn, is sensitive to changes in pressure. Furthermore, one can predict that the higher velocity provoked by raised injection pressure enhances the break-up process, resulting in

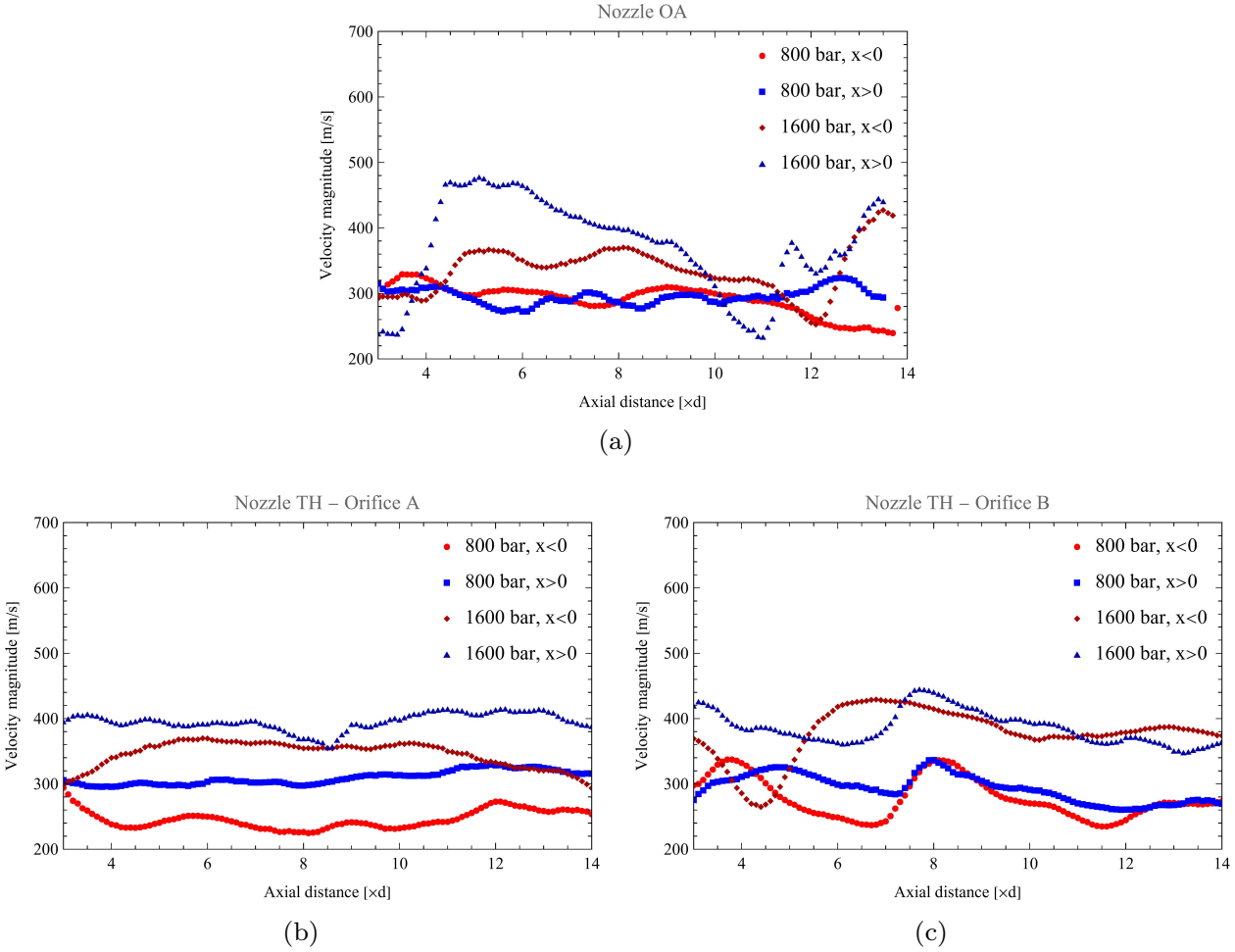

Figure 5.3: *Axial velocity distribution across the spray periphery for a) off-axis nozzle, b) two-hole nozzle orifice A, and c) two-hole nozzle orifice B*

a significant effect on spray characteristics in the far field, such as the maximum liquid penetration length.

Comparing nozzle SH1 with other nozzles indicates that convergent orifices (larger k-factor) generate narrow sprays, while the flow tends to expand more in the radial direction in a cylindrical orifice. According to the results, it is clear that increasing the injection pressure intensifies the spray expansion in nozzle SH1, which is likely due to an increased cavitation level. This matches the trends discussed in Chapter 2, where higher pressure drop and low k-factor are shown to increase the probability of cavitation and its intensity.

The spray profile at a quasi-steady state for the OA nozzle (Figure 5.5(b)) reveals that the spray deviates towards the left side (the side with a sharper inlet edge). This trend is also visible for the second orifice of the TH nozzle (TH-B) but is more gentle. In addition, the overall velocity magnitude on the left side appears to be lower than on the other side. The presence of the sharp edge at the left side probably causes this.

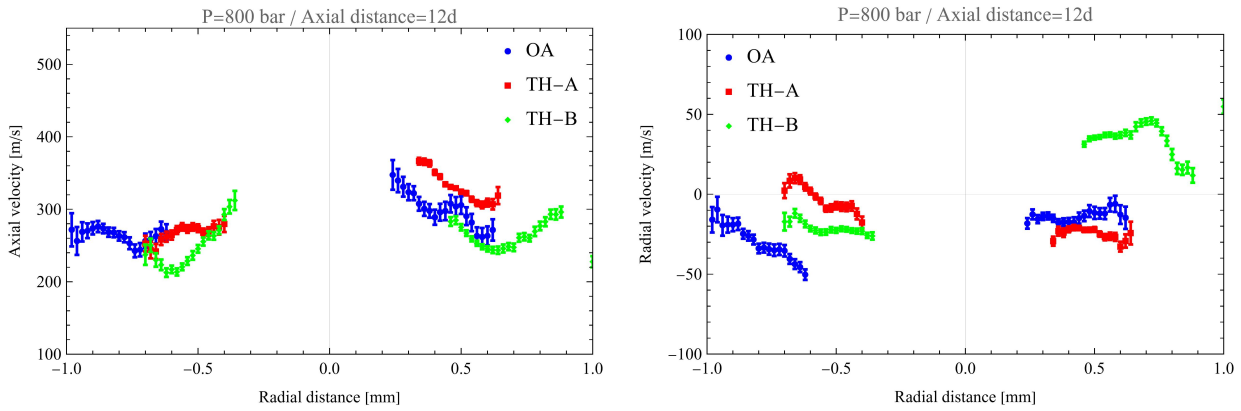

(a) Axial velocity (b) Radial velocity

Figure 5.4: *Axial and radial velocity distribution at 12d distance from the orifice outlet for 3 orifices at 600 μs and 800 bar.*

As mentioned in Chapter 2, cavitation starts with the flow separation from the orifice wall; if an asymmetrical boundary layer forms inside the orifice, a so-called "hydraulic flip" can arise and cause deflection in the spray profile [74]. Therefore, it is likely that a more significant asymmetry at the orifice leads to a more extensive deflection in the spray profile. Moreover, that could be the reason for the lower deviation in spray direction in TH orifices than the OA nozzle (Figure 5.5(b)).

5.2 Statistical analysis and uncertainties

As stated in Chapter 3, we measure the spray kinematics based on 150 to 300 statistical samples. Figure 5.6 shows the aggregation of all extracted velocity magnitudes for spray at 800 μs ASOI and 1600 bar pressure for the OA nozzle. This image is an example to show the non-uniform velocity distribution even in a close neighborhood of any coordinate. Probably shot-to-shot variations in spray profiles and initial conditions, including pressure fluctuations and the amount of residual fuel in the sac, could be the source of variations in velocity magnitudes. In addition, correlation mismatches might also exist, since the correlation coefficient, is never set to 100%. However, the probability of a correlation mismatch is quite low. As mentioned earlier, the velocity magnitude of each point on the spray periphery consists of the mean value of all extracted velocity magnitudes in the neighborhood of that point. Therefore, the reliability of the statistical data needs to be assessed.

To analyze the results, we present them in the form of histograms. As an example, Figure 5.7(a) displays the sample population distribution of all velocities within an 8×8 pixels distance from a random coordinate (x=43, y=321 pixel) at a particular case (800 μs, 1600 bar). At first glance, we notice there is a relatively large range of velocity values and

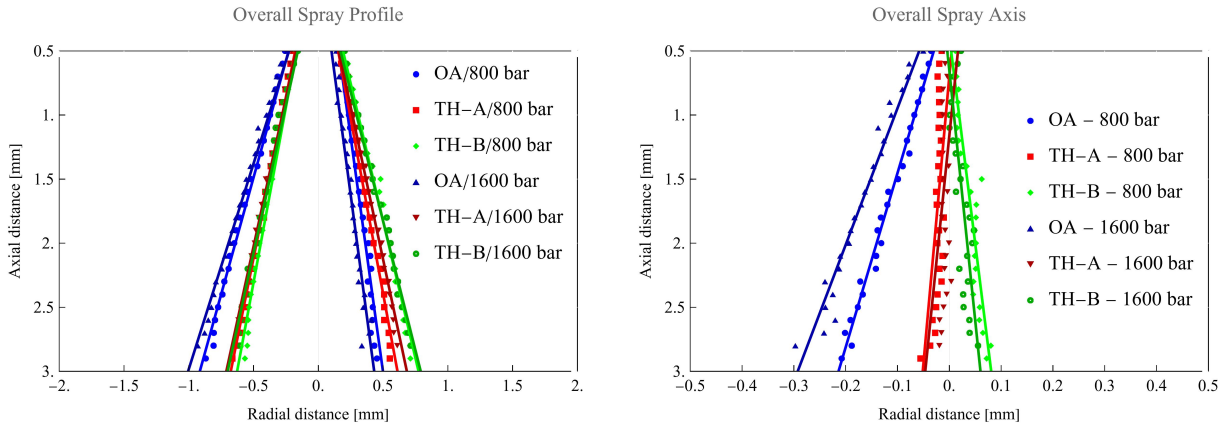

(a) Cone angle (b) Spray axis

Figure 5.5: *Cone angle and spray axis for three nozzles at 600 µs after SOI*

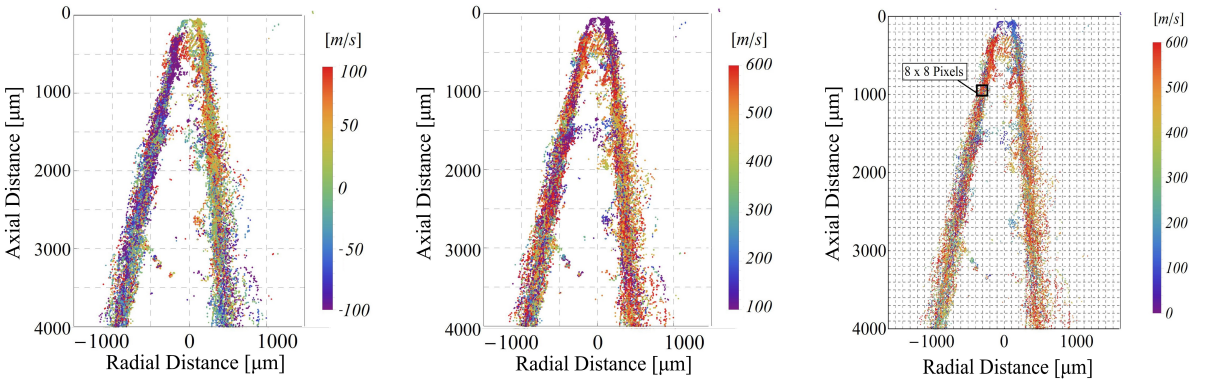

(a) (b) (c)

Figure 5.6: *All extracted velocity data for the OA nozzle at 800 µs after start of injection. a) radial velocity components, b) axial velocity components, and c) velocity magnitudes.*

a large variance. However, the most population exists between 450 to 600 m/s. In order to detect the range with the highest population automatically, we examined the effect of data filtration. Figure 5.7(b) and 5.7(c) depict the histogram of velocity data after mean and median filtering, respectively. Table 5.1 also provides the primary statistical information for each filtering method. These results show that applying median filtering emphasizes the range with the most population, and the calculated average of those data will be closer to the highest population range. In addition, if we eliminate the outliers from the averaging process, the calculated mean (Trimmed mean) will be even placed in the middle of that range. Therefore, we can enhance the obtained results for model validation by applying the median filter.

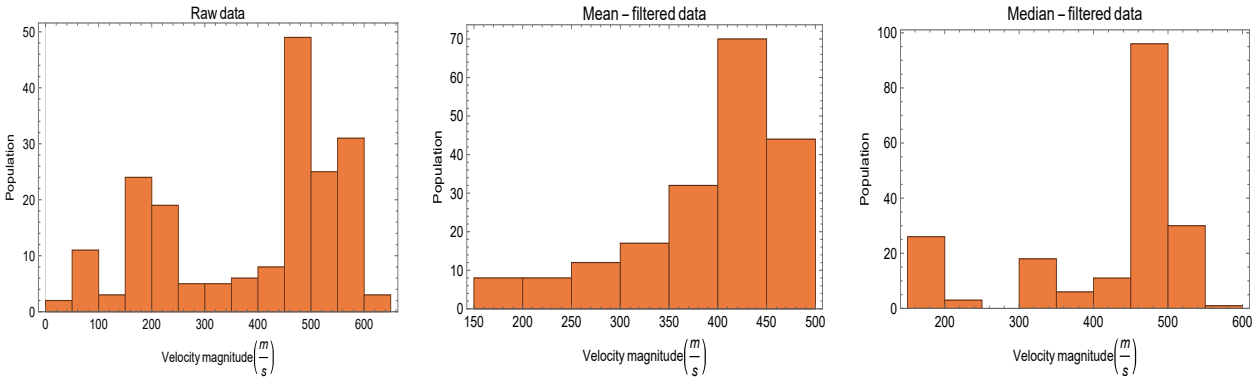

(a) (b) (c)

Figure 5.7: *Histograms of extracted velocity populations for OA nozzle at the coordinate of [43, 321] pixel , 800 µs after start of injection and 1600 bar. a) raw data, b) mean-filtered data, c) median-filterd data.*

Table 5.1: Statistical evaluation of filtering velocity data

Data type	**Mean value [m/s]**	**Median value [m/s]**	**Trimmed mean [m/s]**	**Largest population [m/s]**
Raw	390	445	396	450-500
Mean-filtered	391	419	396	400-450
Median-filtered	416	468	422	450-500

5.3 Model validation analysis

Despite the inherent uncertainties in the experimental dataset and the challenges regarding the data selection, a commendable level of agreement emerges between the experimental measurements and the simulation, particularly when comparing axial velocities. However, when considering the radial components, this agreement appears to be less compelling, possibly due to the statistical complexity involved with the local instabilities associated with radial velocity. In this methodological technique, which includes an assessment of 300 separate sprays, each spray possesses a distinct form. As illustrated in Figure 5.8, one spray can have a bump shape in a particular location while another spray has a depression in the same position. Consequently, at a particular location, a spray shows a positive radial velocity while another registers a negative velocity for the same region. This variance can lead to sections where average velocities tend to converge toward zero.

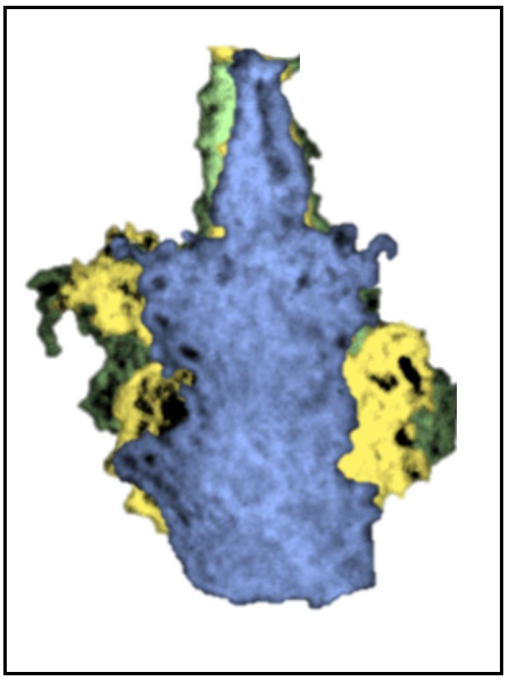

Figure 5.8: *Three sprays with approximately the same penetration length. This figure shows how sprays with similar penetration lengths can be different regarding the radial expansion.*

Conversely, simulation results indicate a periodic alteration in velocity direction throughout the spray. Depending on the spray's penetration length and the elapsed time, a specific point can be set outside of the average window. Thus, when averaging velocities from three sprays with a time difference of 1.5 μs, a point can have both positive and negative velocities, with the result converging toward zero.

Another point to consider is that the model generates broad 3D data, whereas the experimental data are limited to 2D images. This constraint neglects potential motion in the third dimension, parallel to the line of sight, or the spray's swirl motion, which may have an impact on the cross-correlation process.

Finally, the impacts of needle motion were excluded in the simulation model developed in parallel with this study. Considering the internal nozzle flow at 32 μs after SOI (Figure 5.9), the flows from the left and right are in equilibrium. Applying the needle motion effect to the model will probably alter this condition, and this equilibrium condition will not be maintained. In addition, it will impact the near-field spray characteristics as well. Hence, the absence of needle motion in the model is notable, and accounting for this parameter may provide a more accurate picture of the intricate dynamics involved in the spray process, particularly regarding the radial velocity components.

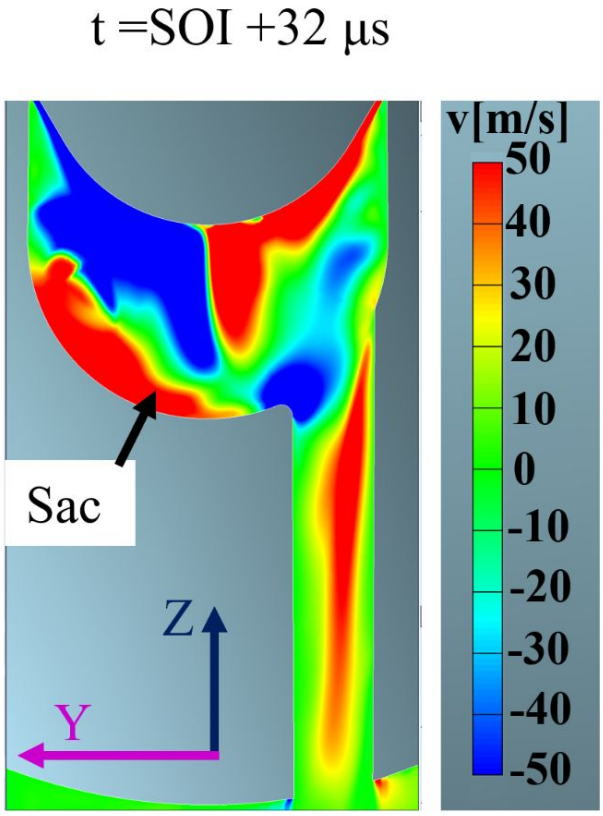

Figure 5.9: *Simulated radial velocity (in Y direction) at 32 µs after SOI*

6 Conclusion and Outlook

6.1 Conclusion

In summary, this project not only revealed profound insights into spray dynamics but also examined how nozzle shape affects spray behavior across a wide range of situations. The research included four nozzles, each with its own set of geometrical characteristics. The experimental design entailed feeding these nozzles to three distinct injection pressures and collecting the spray dynamics at different time instants, including both transient and steady-state conditions. The large dataset, which included measurements from over 70 unique sprays and 35,000 images, allowed for a complete investigation of spray features.

One of the most significant contributions of this study is the extensive evaluation of instantaneous velocities at the spray periphery during selective time steps. This thorough method uncovered nuanced characteristics of spray dynamics, such as instances of acceleration and deceleration in near-field sprays, expanding the understanding of the spray formation process.

The use of statistical spray velocity to validate a simulation model was the main objective of the study, allowing for a better understanding of the delicate interplay between near-field spray characteristics and in-nozzle flow dynamics. The model's effective validation is notable, particularly in terms of obtaining consistency between simulated spray kinematics and experimental velocity data along the axial direction. However, while there is remarkable agreement in the radial directions, deviations exist within some parts of the spatial domain. This highlights the sensitivity of radial velocity components to the statistical approach.

In addition to exploring nozzle geometry, this study delved extensively into the influence of injection pressure. Interestingly, the injection pressure exhibited a negligible effect on the spray profile, except for nozzles more susceptible to cavitation. Instead, its primary contribution manifested in varying spray dynamics, cavitation tendencies, needle opening times, and the timing of spray evolution.

After carrying out the experiments and extensively analyzing the results, it is possible to answer the research questions addressed in Chapter 1.2, as summarized below.

First, the influence of different geometrical features on near-field spray dynamics was investigated. The nozzles studied were characterized by unique geometrical attributes such as outlet diameter, conicity, orifice orientation, and orifice alignment. It was found that a nozzle with a smaller hole diameter produces sprays with a higher overall velocity compared to a nozzle with a larger hole diameter, particularly during the early transient period. This observation aligns with the increased penetration rate observed in sprays from the smaller hole nozzle. Additionally, it was revealed that the velocity of the spray

differs on the two sides of sprays emitted from a nozzle with an asymmetrical orifice inlet, with the side with less flow restriction moving faster. Further investigation showed that while the axial velocity component on the smoother side of the orifice inlet is significantly larger, the radial velocity component is close to zero. A comparison between the velocities of a two-hole nozzle and an off-axis nozzle demonstrated that the two-hole sprays move slower than the off-axis sprays during the very early stage of injection, although this difference diminishes over the steady state.

The study also examined how inlet geometry affects the morphology of the sprays. The most significant geometrical feature observed in the analyzed nozzles and spray profiles was the spray axis. A notable deviation of the spray axis was particularly evident in the off-axis nozzle during the steady state, where the spray deviated towards the side with the sharper orifice inlet. This type of deviation was also detected in one of the two-hole nozzle's orifices. The behavior was investigated in greater depth, with the amount of divergence being calculated under different conditions. It was found that the off-axis spray consistently deviated in a particular direction, with the amount of deviation increasing as the injection pressure rose. Notably, when comparing the spray of TH-B at 600 s to 800 s, the direction of deviation was found to differ, suggesting that the deviation direction may change depending on the stage of injection.

The impact of injection pressure and the sensitivity of certain geometrical parameters to pressure changes were also explored. The experiments considered at least two injection pressure levels. Generally, injection pressure has little impact on the spray profile unless the nozzle has characteristics sensitive to pressure, such as a sharp inlet edge or a low k-factor, which makes the injector more prone to cavitation. This conclusion was drawn from the analysis of SH2 and OA sprays over a range of pressures. The SH2 nozzle, which is nearly cylindrical with a k-factor close to zero, and the OA nozzle, with a sharp edge at the orifice's entrance and a k-factor of approximately 1.4, were found to be critical in terms of cavitation. Both nozzles exhibited significant radial expansion in their spray profiles, with the spray axis deviation of the OA nozzle increasing as pressure increased. Furthermore, higher injection pressure was found to accelerate needle lift within the injector, thereby accelerating spray development and allowing the spray to reach a steady-state condition more quickly, at least in the near-field.

Finally, the study explored the correlation between in-nozzle flow characteristics and near-field spray behavior. After validating the simulation model, internal nozzle flow data for the OA nozzle was analyzed, with a focus on radial and rotational velocities within the nozzle and orifice. The simulation revealed that a separation zone forms at the sharp edge of the orifice, causing the incoming flow to shift to the opposite side of the orifice. This separation results from a combination of rotational and linear motions, leading to counter-rotating flows along the side walls and a linear reciprocating flow in the core region. These combined movements contribute to the radial expansion of the flow, characterized by linear movement in the spray's center and rotational movement on its frontal and rear sides.

6.2 Outlook

This research has made strides in understanding the near-field spray velocity through a statistical approach. While expanding the sample size could further enhance the accuracy and reliability of the data, the findings already offer valuable insights into spray dynamics. Increasing the number of captured images, particularly when aiming for tighter penetration ranges would refine the results even more. Although this process is time-intensive, addressing these challenges in future studies could further deepen the reliability of the velocity distributions obtained.

While the experiments were not conducted under realistic engine operating conditions, the groundwork has been laid for future exploration in this area. The setup of a high-pressure/high-temperature spray chamber provides an exciting opportunity for subsequent research. Investigating the effects of back pressure and ambient temperature on spray dynamics will likely yield new insights and expand the model's applicability. The large window of the new chamber is ideal for far-field observations including the combustion phase and open avenues for studying other spray characteristics such as liquid penetration length, lift-off length, and emissions formation.

As part of this project a new injector holder was designed specifically for the high-pressure/high-temperature chamber and analyzed by finite element tools, which makes another advancement in this project. This design allows the injector to rotate along its axis, enabling the capture of spray images from multiple view angles to create a 360° spray velocity field. This setup, however, applies only to axial-hole nozzles. Future research could leverage this capability to further understand spray behavior, potentially revealing swirl motion and other complex dynamics.

The successful validation of our model for an off-axis nozzle is a major achievement, setting the stage for future work. The next logical step involves modeling a two-hole nozzle and comparing the results with experimental data to assess the model's adaptability to different geometrical constraints. Including needle motion in future modeling efforts could further refine the accuracy of the simulations, as this factor can introduce significant flow disturbances.

Despite areas for further exploration, the most important outcome of this research is the successful validation of the simulation model. This validated model provides a cost-effective and sustainable tool for simulating sprays with varying parameters and nozzle geometries. It holds great promise for combustion engineers, offering a pathway to designing more efficient and environmentally friendly combustion processes, ultimately contributing to reduced emissions and enhanced overall performance.

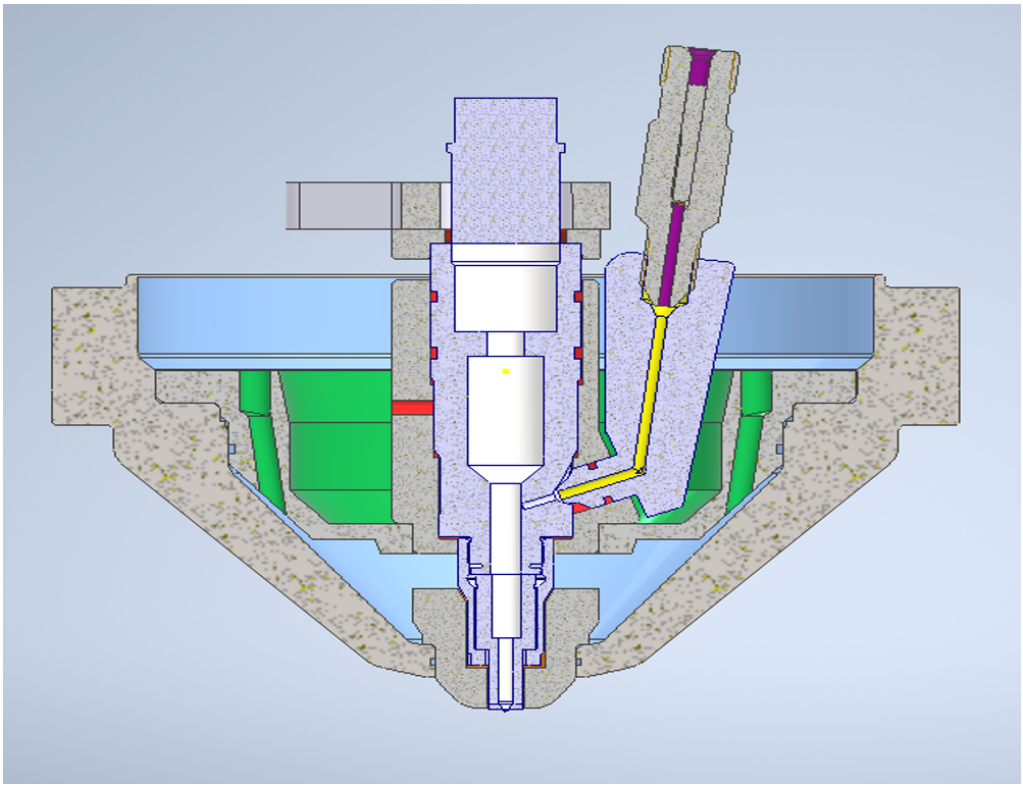

Figure 6.1: *Cross-section view of the injector holder designed for the high-pressure/high-temperature chamber*

Bibliography

[1] Joanna Nowakowska-Grunt and Monika Strzelczyk. “The current situation and the directions of changes in road freight transport in the European Union”. In: *Transportation Research Procedia*. 3rd International Conference "Green Cities – Green Logistics for Greener Cities", Szczecin, 13-14 September 2018 39 (2019).

[2] Ana Carolina Rodrigues Teixeira et al. “Alternative fuel technologies emissions for road heavy-duty trucks: a review”. In: *Environmental Science and Pollution Research* 28.17 (2021).

[3] Arun S. K. Raju, Barry R. Wallerstein, and Kent C. Johnson. “Achieving NOx and Greenhouse gas emissions goals in California’s Heavy-Duty transportation sector”. In: *Transportation Research Part D: Transport and Environment* 97 (2021).

[4] Christopher J. Polonowski et al. “An Experimental Investigation of Low-Soot and Soot-Free Combustion Strategies in a Heavy-Duty, Single-Cylinder, Direct-Injection, Optical Diesel Engine”. In: *SAE International Journal of Fuels and Lubricants* 5.1 (2011).

[5] Gang Li, Chunhua Zhang, and Yangyang Li. “Effects of diesel injection parameters on the rapid combustion and emissions of an HD common-rail diesel engine fueled with diesel-methanol dual-fuel”. In: *Applied Thermal Engineering* 108 (2016).

[6] Wei Chen et al. “Effect of injection strategy on fuel-air mixing and combustion process in a direct injection diesel rotary engine (DI-DRE)”. In: *Energy Conversion and Management* 154 (2017).

[7] S.N. Soid and Z.A. Zainal. “Spray and combustion characterization for internal combustion engines using optical measuring techniques – A review”. In: *Energy* 36.2 (2011). Publisher: Elsevier Ltd.

[8] Sibendu Som et al. “Effect of nozzle orifice geometry on spray, combustion, and emission characteristics under diesel engine conditions”. In: *Fuel* 90.3 (2011). Publisher: Elsevier Ltd.

[9] Safiullah, Keiya Nishida, and Youichi Ogata. “Evaporation and mixture formation characteristics of diesel spray under various nozzle hole size and injection pressure condition employing similar injection rate profile”. In: *International Communications in Heat and Mass Transfer* 123 (2021).

[10] Chengjun Du, Mats Andersson, and Sven Andersson. “Effects of nozzle geometry on the characteristics of an evaporating diesel spray”. In: *SAE International Journal of Fuels and Lubricants* (2016). Publisher: SAE International.

[11] Chunde Yao et al. “Impacts of nozzle geometry on spray combustion of high pressure common rail injectors in a constant volume combustion chamber”. In: *Fuel* 179 (2016). Publisher: Elsevier Ltd.

[12] Ozgur Oguz Taskiran. “Investigation of the effect of nozzle inlet rounding on diesel spray formation and combustion”. In: *Fuel* 217 (2018). Publisher: Elsevier Ltd.

[13] John E. Dec. *A Conceptual Model of DI Diesel Combustion Based on Laser-Sheet Imaging**. SAE Technical Paper 970873. ISSN: 0148-7191, 2688-3627. Warrendale, PA: SAE International, 1997.

[14] Thomas Wintrich and Meike Keller. “Basic principles of diesel fuel injection”. In: *Diesel Engine Management: Systems and Components*. Ed. by Konrad Reif. Wiesbaden: Springer Fachmedien, 2014. ISBN: 978-3-658-03981-3.

[15] Felix Landhäußer et al. “Overview of common-rail systems”. In: *Diesel Engine Management: Systems and Components*. Ed. by Konrad Reif. Wiesbaden: Springer Fachmedien, 2014. ISBN: 978-3-658-03981-3.

[16] Wenbin Yu, Wenming Yang, and Feiyang Zhao. “Investigation of internal nozzle flow, spray and combustion characteristics fueled with diesel, gasoline and wide distillation fuel (WDF) based on a piezoelectric injector and a direct injection compression ignition engine”. In: *Applied Thermal Engineering* 114 (2017). Publisher: Elsevier Ltd.

[17] Ya Gao et al. “Investigation of Needle Motion Profile Effect on Diesel Spray in Near-Nozzle Field”. In: *Micromachines* 13.11 (2022). Publisher: MDPI AG.

[18] Sandro Soccol and Werner Brühmann. “High-pressure components of common-rail system”. In: *Diesel Engine Management: Systems and Components*. Ed. by Konrad Reif. Wiesbaden: Springer Fachmedien, 2014. ISBN: 978-3-658-03981-3.

[19] Arthur H. Lefebvre and Vincent G. McDonell. “Basic Processes in Atomization”. In: *Atomization and Sprays*. 2nd ed. Num Pages: 38. CRC Press, 2017. ISBN: 978-1-315-12091-1.

[20] P. H. Schweitzer. “Mechanism of Disintegration of Liquid Jets”. In: *Journal of Applied Physics* 8.8 (1937).

[21] M. J. McCarthy and N. A. Molloy. “Review of stability of liquid jets and the influence of nozzle design”. In: *The Chemical Engineering Journal*. An International Journal of Research and Development 7.1 (1974).

[22] ROLF DENEYS REITZ. “Atomization and Other Breakup Regimes of a Liquid Jet.” ISBN: 9798661024862. PhD thesis. United States – New Jersey: Princeton University. 336 pp.

[23] Gunnar Stiesch. *Modeling engine spray and combustion processes*. Heat and mass transfer. Springer, 2003. ISBN: 978-3-540-00682-4.

[24] Kuppuraj Rajamanickam, Achintya Mukhopadhyay, and Saptarshi Basu. “On Primary Atomization in Propulsive Device Fuel Injectors—A Short Review”. In: *Droplets and Sprays : Applications for Combustion and Propulsion*. Ed. by Saptarshi Basu et al. Energy, Environment, and Sustainability. Singapore: Springer, 2018. ISBN: 978-981-10-7449-3.

[25] Luka Lešnik et al. “The influence of in-nozzle cavitation on flow characteristics and spray break-up”. In: *Fuel* 222 (2018).

[26] Zhou Chen et al. “Experimental study on the effect of nozzle geometry on string cavitation in real-size optical diesel nozzles and spray characteristics”. In: *Fuel* 232 (2018). Publisher: Elsevier Ltd.

[27] F. Payri et al. “A contribution to the understanding of cavitation effects in Diesel injector nozzles through a combined experimental and computational investigation”. In: *Computers & Fluids* 58 (2012).

[28] Chengjun Du, Sven Andersson, and Mats Andersson. “The effect of cavitation on the estimation of fuel injection rates based on momentum flux measurements”. In: *Fuel* 238 (2019). Publisher: Elsevier Ltd.

[29] F.J. Salvador et al. “Comparison of microsac and VCO diesel injector nozzles in terms of internal nozzle flow characteristics”. In: *Energy Conversion and Management* 103 (2015). Publisher: Elsevier Ltd.

[30] S. Molina et al. “A computational investigation on the influence of the use of elliptical orifices on the inner nozzle flow and cavitation development in diesel injector nozzles”. In: *Energy Conversion and Management* 79 (2014). Publisher: Elsevier Ltd.

[31] J. Javier López et al. “A comprehensive study on the effect of cavitation on injection velocity in diesel nozzles”. In: *Energy Conversion and Management*. IREC 2011, The International Renewable Energy Congress 64 (2012).

[32] Byunggyun Kim and Suhan Park. “Study on in-nozzle flow and spray behavior characteristics under various needle positions and length-to-width ratios of nozzle orifice using a transparent acrylic nozzle”. In: *International Journal of Heat and Mass Transfer* 143 (2019). Publisher: Elsevier Ltd.

[33] Zhixia He et al. “Study of the effect of nozzle hole shape on internal flow and spray characteristics”. In: *International Communications in Heat and Mass Transfer* 71 (2016). Publisher: Elsevier Ltd.

[34] Guangjun Jiang et al. “Study of the generated density of cavitation inside diesel nozzle using different fuels and nozzles”. In: *Energy Conversion and Management* 103 (2015). Publisher: Elsevier Ltd.

[35] Z. He et al. “Visual experiment of transient cavitating flow characteristics in the real-size diesel injector nozzle”. In: *International Communications in Heat and Mass Transfer* 78 (2016). Publisher: Elsevier Ltd.

[36] Ming-Chia D Lai Philip J Dingle. *Diesel Common Rail and Advanced Fuel Injection Systems*. SAE International, 2005. ISBN: 978-0-7680-2200-1.

[37] Fujun Wang and Tiegang Fang. “Liquid jet breakup for non-circular orifices under low pressures”. In: *International Journal of Multiphase Flow* 72 (2015). Publisher: Elsevier Ltd.

[38] Shenghao Yu et al. “Internal flow and spray characteristics for elliptical orifice with large aspect ratio under typical diesel engine operation conditions”. In: *Fuel* 228 (2018). Publisher: Elsevier Ltd.

[39] Kuibin Zhou et al. “Effect of nozzle exit shape on the geometrical features of horizontal turbulent jet flame”. In: *Fuel* 260 (2020). Publisher: Elsevier Ltd.

[40] Chen Chen et al. “Investigation of inner flow and near-field spray patterns of the non-circular diesel injector”. In: *Sadhana-Academy Proceedings in Engineering Sciences* 47.1 (2022).

[41] F. J. Salvador et al. “Analysis of the combined effect of hydrogrinding process and inclination angle on hydraulic performance of diesel injection nozzles”. In: *Energy Conversion and Management* 105 (2015).

[42] Hadi Taghavifar, Mohammad Taghi Shervani-Tabar, and Majid Abbasalizadeh. “Numerical study of the effects of injector needle movement and the nozzle inclination angle on the internal fluid flow and spray structure of a group-hole nozzle layout”. In: *Applied Mathematical Modelling* 39.23 (2015). Publisher: Elsevier Inc.

[43] Fuying Xue et al. “Numerical analyses of transient flow characteristics within each nozzle hole of an asymmetric diesel injector”. In: *International Journal of Heat and Mass Transfer* 104 (2017). Publisher: Elsevier Ltd.

[44] F.J. Salvador et al. “Experimental investigation of the effect of orifices inclination angle in multihole diesel injector nozzles. Part 1 – Hydraulic performance”. In: *Fuel* 213 (2018). Publisher: Elsevier Ltd.

[45] R. Payri et al. “Experimental investigation of the effect of orifices inclination angle in multihole diesel injector nozzles. Part 2 – Spray characteristics”. In: *Fuel* 213 (2018). Publisher: Elsevier Ltd.

[46] Raul Payri et al. “A study of the relation between nozzle geometry, internal flow and sprays characteristics in diesel fuel injection systems”. In: *Journal of Mechanical Science & Technology* 18.7 (2004).

[47] Raul Payri et al. “The effect of nozzle geometry over internal flow and spray formation for three different fuels”. In: *Fuel* 183 (2016). Publisher: Elsevier Ltd.

[48] J. Cui et al. “Quantitative analysis of the minor deviations in nozzle internal geometry effect on the cavitating flow”. In: *Experimental Thermal and Fluid Science* 94 (2018). Publisher: Elsevier Inc.

[49] Chenglong Tang et al. “Experimental study on the effect of injector nozzle K factor on the spray characteristics in a constant volume chamber: Near nozzle spray initiation, the macroscopic and the droplet statistics”. In: *Fuel* 202 (2017).

[50] Zuo-Yu Sun et al. “Numerical investigation on effects of nozzle’s geometric parameters on the flow and the cavitation characteristics within injector’s nozzle for a high-pressure common-rail DI diesel engine”. In: *Energy Conversion and Management* 89 (2015).

[51] Seoksu Moon et al. “Near-field dynamics of high-speed diesel sprays: Effects of orifice inlet geometry and injection pressure”. In: *Fuel* 133 (2014). Publisher: Elsevier Ltd.

[52] Yu Jin et al. “Comparison of diesel spray with small injection amount between single-hole and multi-hole injectors: Results under same rail pressure and similar injection rate”. In: *International Communications in Heat and Mass Transfer* 118 (2020).

[53] Weidi Huang et al. “Eccentric needle motion effect on near-nozzle dynamics of diesel spray”. In: *Fuel* 206 (2017).

[54] P. Dong et al. “Characteristics of the internal flow and the near-field spray of a single-hole injector and a multi-hole injector for diesel engines”. In: *Proceedings of the Institution of Mechanical Engineers, Part D: Journal of Automobile Engineering* 230.5 (2016). Publisher: SAGE Publications Ltd.

[55] Seoksu Moon et al. “Effect of the number and position of nozzle holes on in- and near-nozzle dynamic characteristics of diesel injection”. In: *Fuel* 150 (2015). Publisher: Elsevier Ltd.

[56] Safiullah et al. “Effects of full transient Injection Rate and Initial Spray Trajectory Angle profiles on the CFD simulation of evaporating diesel sprays- comparison between singlehole and multi hole injectors”. In: *Energy* 263 (2023). Publisher: Elsevier Ltd.

[57] Yijie Wei et al. “Time-resolved measurement of the near-nozzle air entrainment of high-pressure diesel spray by high-speed micro-PTV technique”. In: *Fuel* 268 (2020).
[58] Meshack Hawi et al. “Effect of injection pressure and ambient density on spray characteristics of diesel and biodiesel surrogate fuels”. In: *Fuel* 254 (2019).
[59] Balaji Mohan et al. “Macroscopic spray characterization under high ambient density conditions”. In: *Experimental Thermal and Fluid Science* 59 (2014).
[60] F. J. Salvador et al. “Experimental analysis of the injection pressure effect on the near-field structure of liquid fuel sprays”. In: *Fuel* 292 (2021).
[61] Raditya Hendra Pratama, Weidi Huang, and Seoksu Moon. “Unveiling needle lift dependence on near-nozzle spray dynamics of diesel injector”. In: *Fuel* 285 (2021).
[62] Graham Pitcher, Graham Wigley, and Mark Saffman. “Velocity and Drop Size Measurements in Fuel Sprays in a direct injection diesel engine”. In: *Particle & Particle Systems Characterization* 7.1 (1990).
[63] Z.-M. Cao et al. “PIV measurement of internal structure of diesel fuel spray: Experiments in Fluids”. In: *Experiments in Fluids* 29.7 (2000).
[64] Cossali Gianpietro E., Brunello Gianni, and Coghe Aldo. *LDV Characterization of Air Entrainment in Transient Diesel Sprays*. 0148-7191. 400 Commonwealth Drive, Warrendale, PA, United States: SAE International, 1991.
[65] Stephane Roux, Francois Hild, and Yves Berthaud. “Correlation image velocimetry: a spectral approach: Applied Optics”. In: *Applied Optics* 41.1 (2002). Publisher: Optical Society of America.
[66] David Sedarsky et al. “Fast-framing ballistic imaging of velocity in an aerated spray”. In: *Optics Letters* 34.18 (2009).
[67] David Sedarsky et al. “Velocity measurements in the near field of a diesel fuel injector by ultrafast imagery”. In: *Experiments in Fluids* 54.2 (2013). arXiv: 1301.6593.
[68] Mark A. Linne et al. “Ballistic imaging of liquid breakup processes in dense sprays”. In: *Proceedings of the Combustion Institute* 32.2 (2009).
[69] Lyle M. Pickett et al. “Comparison of Near-Field Structure and Growth of a Diesel Spray Using Light-Based Optical Microscopy and X-Ray Radiography”. In: *SAE International Journal of Engines* 7.2 (2014).
[70] Zachary Falgout et al. “Gas/fuel jet interfaces under high pressures and temperatures”. In: *Fuel* 168 (2016).
[71] Harsh Purwar et al. “Collinear, two-color optical Kerr effect shutter for ultrafast time-resolved imaging”. In: *Optics Express* 22.13 (2014). arXiv: 1502.03350.
[72] David Sedarsky et al. “Planar velocity analysis of diesel spray shadow images”. In: *arXiv:1203.5347 [physics]* (2012). arXiv: 1203.5347.
[73] Cyril Crua, Morgan R. Heikal, and Martin R. Gold. “Microscopic imaging of the initial stage of diesel spray formation”. In: *Fuel* 157 (2015).
[74] Celia Soteriou, Richard Andrews, and Mark Smith. “Direct Injection Diesel Sprays and the Effect of Cavitation and Hydraulic Flip on Atomization”. In: International Congress & Exposition. 1995.

Abbreviations

$ASOI$	After the Start Of Injection
BI	Ballistic Imaging
CFD	Computational Fluid Dynamics
CI	Compression Ignition
CO	Carbon monoxide
$CO2$	Carbon dioxide
D	Orifice Diameter
HC	Hydrocarbon
HPC	High Pressure Connector
$HSOI$	Hydraulic Start Of Injection
$ICCD$	Intensified Charge-Coupled Device
L	Orifice Length
NOx	Nitrogen Oxides
OA	Off-Axis nozzle
Oh	Ohnesorge Number
OKE	Optical Kerr Effect
PIV	Particle Image Velocimetry
$PLIF$	Planar Laser Induced Fluorescence
Re	Reynolds Number
$SH1$	Single-Hole nozzle 1
$SH2$	Single-Hole nozzle 2
SI	Spark Ignition
SMD	Sauter Mean Diameter
SOI	Start of Injection
$TH-A$	Two-Hole nozzle- orifice A
$TH-B$	Two-Hole nozzle- orifice B
TH	Two-Hole nozzle
We	Weber Number
XPI	eXtra high Pressure Injection